UC Riverside
UC Riverside Previously Published Works

Title

METTL13 Methylation of eEF1A Increases Translational Output to Promote Tumorigenesis

Permalink

https://escholarship.org/uc/item/0fn1714s

Journal

Cell, 176(3)

ISSN

0092-8674

Authors

Liu, Shuo
Hausmann, Simone
Carlson, Scott Moore
et al.

Publication Date

2019

DOI

10.1016/j.cell.2018.11.038

Peer reviewed

METTL13 methylation of eEF1A increases translational output to promote tumorigenesis

Shuo Liu[#1], **Simone Hausmann**[#2], **Scott Moore Carlson**[1], **Mary Esmeralda Fuentes**[2], **Joel William Francis**[1], **Renjitha Pillai**[3], **Shane Michael Lofgren**[2], **Laura Hulea**[4], **Kristofferson Tandoc**[4], **Jiuwei Lu**[5], **Ami Li**[6], **Nicholas Dang Nguyen**[2], **Marcello Caporicci**[2], **Michael Paul Kim**[7], **Anirban Maitra**[8], **Huamin Wang**[8,9], **Ignacio Ivan Wistuba**[8,10], **John Anthony Porco Jr.**[11], **Michael Cory Bassik**[6], **Joshua Eric Elias**[12], **Jikui Song**[5], **Ivan Topisirovic**[4], **Capucine Van Rechem**[3], **Pawel Karol Mazur**[2,#], and **Or Gozani**[1,13,#]

[1]Department of Biology, Stanford University, Stanford, CA 94305, USA

[2]Department of Experimental Radiation Oncology, The University of Texas MD Anderson Cancer Center, Houston, TX, 77030, USA

[3]Department of Pathology, Stanford University School of Medicine, Stanford, CA 94305, USA

[4]Lady Davis Institute and Gerald Bronfman Department of Oncology, McGill University, Montreal, Quebec H3T 1E2, Canada

[5]Department of Biochemistry, University of California, Riverside, CA 92521, USA

[6]Department of Genetics, Stanford University School of Medicine, Stanford, CA 94305, USA

[7]Department of Surgical Oncology, The University of Texas MD Anderson Cancer Center, Houston, TX, 77030, USA

[8]Department of Translational Molecular Pathology, The University of Texas MD Anderson Cancer Center, Houston, TX, 77030, USA

[9]Department of Pathology, The University of Texas MD Anderson Cancer Center, Houston, TX, 77030, USA

[10]Department of Thoracic/Head and Neck Medical Oncology, The University of Texas MD Anderson Cancer Center, Houston, TX, 77030, USA

Publisher's Disclaimer: This is a PDF file of an unedited manuscript that has been accepted for publication. As a service to our customers we are providing this early version of the manuscript. The manuscript will undergo copyediting, typesetting, and review of the resulting proof before it is published in its final citable form. Please note that during the production process errors may be discovered which could affect the content, and all legal disclaimers that apply to the journal pertain.

[11]Department of Chemistry, Boston University, Boston, MA 02215, USA

[12]Deparment of Chemical and Systems Biology, Stanford University School of Medicine, Stanford CA 94305, USA

[13]Lead contact

[#] These authors contributed equally to this work.

Summary

Increased protein synthesis plays an etiologic role in diverse cancers. Here we demonstrate that METTL13 (methyltransferase-like 13) dimethylation of eEF1A (eukaryotic elongation factor 1A) lysine 55 (eEF1AK55me2) is utilized by Ras-driven cancers to increase translational output and promote tumorigenesis *in vivo*. METTL13-catalyzed eEF1A methylation increases eEF1A's intrinsic GTPase activity *in vitro* and protein production in cells. METTL13 and eEF1AK55me2 levels are upregulated in cancer and negatively correlate with pancreatic and lung cancer patient survival. METTL13 deletion and eEF1AK55me2 loss dramatically reduce Ras-driven neoplastic growth in mouse models and in patient-derived xenografts (PDX) from primary pancreatic and lung tumors. Finally, METTL13 depletion renders PDX tumors hypersensitive to drugs that target growth-signaling pathways. Together, our work uncovers a mechanism by which lethal cancers become dependent on the METTL13-eEF1AK55me2 axis to meet their elevated protein synthesis requirement and suggests that METTL13 inhibition may constitute a targetable vulnerability of tumors driven by aberrant Ras-signaling.

Graphical Abstract:
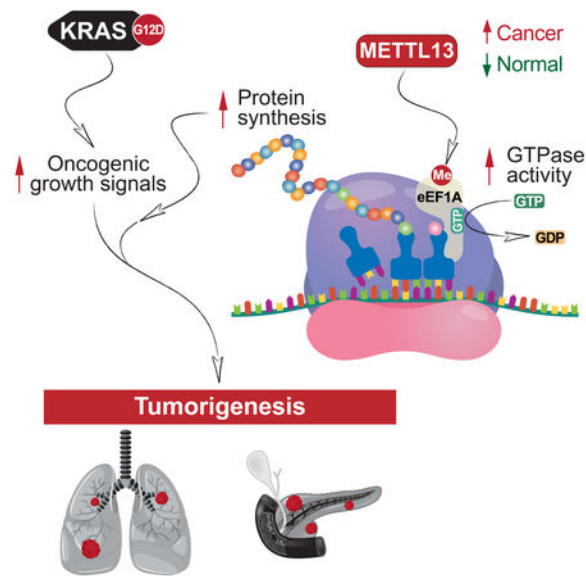
Keywords

METTL13; eEF1A; lysine methylation; RAS; protein methylation; translation; translation elongation; pancreatic cancer; lung cancer

Introduction

Lysine methylation is the addition of one, two or three methyl groups to the ε-nitrogen of a lysine sidechain, forming mono-, di-, and tri-methylated derivatives (referred to here as me1, me2, and me3, respectively). The chemical addition of methyl moieties to lysine residues is catalyzed by lysine methyltransferases (KMTs). Biological functions for lysine methylation is best characterized on histone proteins and the regulation of epigenetics and chromatin biology (Chi et al., 2010). Beyond histones, there is a growing appreciation that a number of non-histone proteins (e.g. p53, RB, RelA) are modulated by lysine methylation (Carlson and Gozani, 2016). In the human proteome there are predicted to be greater than 100 KMTs that belong to one of two protein methylase families: SET (Su(var)3–9, Enhancer-of-zeste, Trithorax) domain enzymes and 7bS (seven-β-strand) enzymes (Clarke, 2013). All of the validated histone KMTs reside within the SET domain family with the exception of the H3K79 KMT hDOT1L, which belongs to the 7βS family. Several additional SET and 7βS enzymes methylate non-histone proteins to influence different nuclear and cytoplasmic activities; however, the biological function, catalytic activity and substrate specificity for the majority of the large family of 7βS KMTs remains to be elucidated (Carlson and Gozani, 2016).

The GTPase eEF1A (eukaryotic elongation factor 1 alpha) is an evolutionarily conserved and fundamental non-ribosomal component of the translational machinery and one of the most abundant proteins found in eukaryotic proteomes (Schuller and Green, 2018). Methylation of eEF1A occurs at several lysine residues, many of which are conserved from yeast to humans (Hamey and Wilkins, 2018; Jakobsson et al., 2018a). Further, it has been suggested that akin to the extensive role histone methylation plays in chromatin regulation, eEF1A methylation may likewise regulate distinct eEF1A-mediated biology, including translation elongation. In humans, there are two eEF1A paralogs, eEF1A1 and eEF1A2, which are 90% identical and 98% similar. The expression of eEF1A1 is ubiquitous while eEF1A2 expression is limited largely to post-mitotic cells (e.g. neurons and cardiomyocytes) (Lee and Surh, 2009). However, eEF1A2 expression is re-activated in cancers and eEF1A1 levels are generally higher in neoplastic relative to normal tissues (Lee and Surh, 2009). Furthermore, cancers that are driven by PI3K-AKT activation show increased sensitivity to eEF1A inhibitors (Lee and Surh, 2009). Connections between mRNA translation and cancer are well-established whereby it is postulated that alterations in the components of the translation apparatus, including eEF1A1/2 overexpression, may be required to fuel neoplastic growth downstream of oncogenic RAS-MAPK and PI3K-AKT signaling, which frequently drive lethal neoplasms including lung and pancreatic cancer (Bhat et al., 2015; Robichaud et al., 2018; Truitt and Ruggero, 2016).

Lung cancer is the most common cause of global cancer-related mortality, leading to over a million deaths each year, and lung adenocarcinoma (LAC) is the most common histological type. Most LAC cases are due to oncogenic KRAS and/or additional mutations that are to date unfortunately not clinically actionable. Pancreatic cancer is also a lethal malignancy. More than 75% of patients die within the first twelve months of diagnosis; the five-year survival rate is below 5%. Pancreatic ductal adenocarcinoma (PDAC) is the most prevalent pancreatic cancer subtype. It typically presents at an advanced stage and is refractory to

most treatment modalities. The vast majority of PDAC cases express oncogenic mutant KRAS (Almoguera et al., 1988). Due to the lethality of LAC and PDAC, the fundamental role of the KRAS pathway, and the difficulty in directly inhibiting KRAS, drug discovery efforts have turned to inhibiting downstream kinase targets (e.g. RAF, MEK1/2 and ERK1/2) and Ras-activated pathways (e.g. PI3K). While compounds that inhibit these kinases have shown promise in cell culture and animal experiments, clinical studies have been less encouraging due to toxicity and the development of therapy resistance (Infante et al., 2014). Thus, there is great interest in identifying factors that cooperate with the canonical KRAS pathway to drive cancer with the hope that a therapeutic strategy hitting multiple pathways will hinder resistance development, while also mitigating toxicity by lowering the overall dose needed for each medicine.

In this work, we find that di-methylation of eEF1A at lysine 55 (eEF1AK55me2) is a high stoichiometry species that is upregulated in pancreatic and lung cancers and associated with poor clinical outcomes. In a genetic screen we identify the orphan protein METTL13 as the physiologic enzyme specifically tasked with generating eEF1AK55me2. Notably, METTL13 expression is also upregulated in cancer wherein it negatively correlates with patient survival. We demonstrate that METTL13, *via* eEF1AK55 methylation, regulates protein synthesis in cancer cells. Further, METTL13 depletion inhibits proliferation of several cancer cell lines and significantly reduces tumorigenesis *in vivo* in Ras-driven pancreatic and lung cancer mouse models and in patient-derived xenograft models from human pancreatic and lung cancers. Finally, we show that METTL13 depletion markedly sensitizes cancer cells and xenograft tumors to drugs that target growth-signaling pathways. Together, our data support a model in which regulation of translation elongation by the METTL13-eEF1AK55me2 axis serves as a mechanism utilized by malignancies to adapt to their increased translational requirements.

RESULTS

Identification of the orphan gene METTL13 as a candidate eEF1A lysine 55 dimethyltransferase

The methylation of eEF1A is conserved from yeast to humans, suggesting that akin to histone methylation, a modification network may regulate specific eEF1A functions (Hamey and Wilkins, 2018; Jakobsson et al., 2018a). While several conserved enzymes that methylate different residues on eEF1A have been identified, the KMT responsible for generating methylation of eEF1A at lysine 55 (eEF1AK55me), a modification that is present in humans but not detected in yeast, is not known (Figure 1A). We analyzed methylation of eEF1A purified from seven cell lines by liquid chromatography tandem mass spectrometry (LC-MS/MS) and found that >98% of eEF1A1/2 molecules harbor di-methylation at K55, with a small fraction of K55 being unmodified or bearing mono-methylation (Figure 1B and S1A-B). Next, we raised state-specific eEF1AK55me1–3 antibodies and found that each antibody selectively recognized its own state of methylation on eEF1A peptides (Figure 1C and S1C). In addition, the anti-eEF1AK55me2 antibody selectively recognized eEF1AK55me2 peptides, as it did not bind to 19 different peptides from other proteins that harbour a dimethyl lysine (Figure S1D).

To discover the enzyme that generates the eEF1AK55me2 mark, we used a gene editing coupled biochemical screening strategy (see schematic, Figure 1D). 107 known and putative KMTs in the human genome were identified and a focused CRISPR/Cas9 knockout collection was generated consisting of 3 independent small guide RNAs (sgRNA) per KMT gene and one control sgRNA for a total of 322 sgRNAs (Table S1). The collection was used to generate 322 individual U2OS cell lines, each expressing a single sgRNA from the collection. Lysates were prepared from each individual cell line to generate a collection of 322 unique lysates, which were systematically probed with the eEF1AK55me2 antibody to determine gene(s) whose deletion results in loss of the eEF1A methylation signal (Figure 1D; for control lysate see Figure S1E). Strikingly, out of the 107 potential KMTs that were targeted by sgRNAs, abrogating *METTL13* expression was the only intervention that reduced eEF1AK55me2 signal (Figure S1E-F). Notably, two sgRNAs (METTL13-b and -c) reduced METTL13 protein levels, which was paralleled by a decrease in eEF1AK55me2 signal, whereas cells expressing the METTL13-a sgRNA retained METTL13 expression and failed to reduce eEF1AK55me2 signal (Figure 1E). These results suggest that out of 107 potential KMTs in the human genome, only METTL13, an uncharacterized member of the 7βS family, regulates eEF1AK55 dimethylation in U2OS cells.

The principal physiologic activity of METTL13 is generation of eEF1AK55me2

In *in vitro* methylation assays using recombinant proteins with ^{3}H-SAM (*S*-adenosyl-methionine) as the methyl donor, METTL13 methylated GST-eEF1A1 and GST-eEF1A2, but not eEF1A1/2 proteins harboring a K55R substitution (Figure 2A). We also performed *in vitro* methylation reactions with non-radiolabeled SAM and observed METTL13 mono- and dimethylation (but not tri-methylation) of eEF1A1/2 at K55 by Western blotting (Figure 2B) and LC-MS/MS (Figure S2A-B).

METTL13 contains two putative methyltransferase (MTase) domains, one at the N-terminus and one at the C-terminus (top panel, Figure 2C). The N-terminal MTase 1 domain is necessary for METTL13 methylation of GST-eEF1AK55, whereas the C-terminal domain is dispensable for this activity (Figure 2C). Structure-function analysis identified residues 1-401 of METTL13 as sufficient for eEF1AK55 methylation activity, as further C-terminal deletions were not tolerated (Figure 2D). Using a combination of structural modelling (Figure S2C) and sequence homology to other 7βS KMTs (Figure S2D), we identified several specific substitutions that abrogated METTL13's catalytic activity (Figure S2D), including G58R, which is predicted to interfere with SAM binding (Figure 2E and S2C).

In addition to U2OS cells (see Figure 1E), we found that depletion of METTL13 by two independent sgRNAs (targeting exon-intron junctions and named METTL13-1 and METTL13-2) resulted in loss of eEF1AK55me2 in six additional cell lines as determined by Western blotting (Figure 3A; LC-MS/MS shown in Figure S3A). Complementation of METTL13-depleted NCI-H2170 cells with CRISPR-resistant wild-type METTL13, but not the catalytic-dead METTL13$_{G58R}$, restored eEF1AK55me2 levels (Figure 3B). Collectively, these results identify METTL13 as a bona fide KMT that methylates eEF1A at K55 *in vitro* and is required for maintenance of physiologic levels of eEF1AK55me2 in cells in a catalytic activity-dependent manner.

eEF1A is one of the more abundant proteins in the human proteome and K55me2 is a high-stoichiometry event (Hamey and Wilkins, 2018; Jakobsson et al., 2018a) (Figure 1B). Based on our screen (Figure S1F) and cellular depletion studies (Figure 3A), our data argue that METTL13 is the principal enzyme tasked with generating physiologic eEF1AK55me2. This raises the question of whether the converse is true: is eEF1AK55 the only METTL13 substrate or one of many relevant substrates? Histones are heavily methylated and there are many enzymes that function as histone KMTs (Mum and Shi, 2017). However, *in vitro,* METTL13 does not methylate the four core histones (H3, H2A, H2B, and H4) or nucleosomes (Figure 3C). In addition, METTL13 does not methylate any proteins present in the 40S and 60S ribosomal subunits and 80S ribosomes that lack eEF1A (Figures 3D and S3B). To investigate METTL13 catalytic specificity in a physiologic and unbiased setting, we used quantitative proteomics to compare the methylome of the PDAC cell line T3M4 ±METTL13 (Figure 3E). Of the >1000 methylation events detected in the analysis, eEF1AK55 methylation (me1 and me2) were the only modifications quantitatively altered upon METTL13 depletion; no changes were observed in histone methylation or for other eEF1A methylated residues (Figure 3E; Table S2). Structural modeling of the METTL13 catalytic core showed a distinct substrate recognition domain (Figure S2C), which is reminiscent of PrmA, a bacterial lysine methyltransferase that achieves substrate specificity through a conformation-specific enzyme-substrate interaction (Demirci et al., 2007). Indeed, METTL13 requires full-length eEF1A and is not active on an eEF1A peptide spanning K55 of eEF1A (Figure S3C), suggesting that it employs a three-dimensional topological substrate recognition mechanism similar to that of PrmA. Taken together, these results indicate that the principal physiologic catalytic activity of METTL13 is eEF1AK55 methylation (see Discussion).

METTL13 and eEF1AK55me2 are highly expressed in pancreatic cancer and promote proliferation of pancreatic cancer cells.

A meta-analysis of six publicly available human PDAC datasets showed consistent up-regulation of *METTL13* mRNA levels and a significant negative correlation between high METTL13 expression and PDAC patient survival (Figures S4A-B). Moreover, while METTL13 protein expression was largely undetected by immunohistochemistry (IHC) in the normal pancreas, it was clearly observed in sections from murine and human PDAC samples (Figure 4A and S4C). IHC analysis of eEF1AK55me2 signal also showed a similar pattern, with low signal in normal pancreas and a strong signal in adjacent malignant tissue (Figure 4A and S4C). Further, both METTL13 and eEF1AK55me2 immunostaining signals on PDAC patient tissue arrays showed significant correlation with poor patient survival (Figure 4B-C). Similar results were observed for METTL13 expression and eEF1AK55me2 signal in lung cancer (Figures S4D-F). Consistent with these results, there is a strong correlation between METTL13 and eEF1AK55me2 protein levels in both cancer types (Figure 4D). Finally, METTL13 and eEF1AK55me2 (and total eEF1A) levels are all elevated in pancreatic and lung cancer cell lines compared to the non-transformed IMR-90 and RPE-1 cell lines (Figure 4E).

Our observations suggest a potential role for METTL13 and eEF1AK55me2 in oncogenesis. In this regard, depletion of METTL13 had no impact on proliferation of the non-transformed

RPE-1 cell line (Figure 4F) but inhibited proliferation of the PDAC T3M4 cell line (Figure 4G) and six additional pancreatic, lung and other cancer cell lines (Figure S4G). The reduction in proliferation upon METTL13 depletion in T3M4 cells was rescued by complementation with CRISPR-resistant ectopic wild-type METTL13, but not by complementation with catalytically inactive METTL13$_{G58R}$ (Figure 4H). Our results implicate METTL13 methylation of eEF1AK55 in PDAC cell proliferation. We next wanted to independently test the role of eEF1AK55 in the regulation of T3M4 cell proliferation. Since the highly abundant eEF1A1 isoform of eEF1A is essential for mRNA translation and eEF1A2 expression is re-activated in cancers, we focused on testing K55 in the context of eEF1A2 function in proliferation. Depletion of eEF1A2 led to a moderate reduction in overall eEF1AK55me2 levels (with the likely remaining signal being chiefly eEF1A1K55me2) and moderately attenuated proliferation of T3M4 cells (Figure 4I). Complementation with wild-type eEF1A2, but not eEF1A2 harboring a K55R substitution (eEF1A2$_{K55R}$), was able to fully restore cancer cell proliferation (Figure 4I). Together these data argue that METTL13 regulates the proliferation of pancreatic cancer cells *via* di-methylation of eEF1AK55.

Methylation regulates eEF1A GTPase activity and mRNA translation in cells

Since K55 of eEF1A is located on the catalytic surface of the eEF1A GTPase domain, we investigated the possibility that methylation may modulate its GTPase activity. To this end, recombinant Flag-tagged eEF1A proteins ±K55me were purified from either METTL13-overexpressing 293T cells or METTL13-depleted 293T cells expressing METTL13$_{G58R}$ (leading to virtually complete loss of K55 methylation) (Figures 5A and S5A). We performed *in vitro* GTP hydrolysis assays to determine Michaelis-Menten kinetic properties of purified eEF1A proteins ± K55me2 (Figure S5B). The catalytic efficiency (k_{cat}/K_M) of eEF1A was ~20% higher in the K55 methylated state relative to the unmethylated state (Figure 5B and S5B), due to an increase in V_{max} with no change in the Michaelis constant (Figure 5B). Notwithstanding that K55 dimethylation increased basal GTPase activity of eEF1A, aminoacyl-tRNAs (aa-tRNAs) stimulation of eEF1A GTPase activity did not depend on the K55 methylation status (Cavallius and Merrick, 1998; Van Noort et al., 1986) (Figure S5C). Though upon aa-tRNA stimulation, GTPase activity of K55 dimethylated eEF1A remained higher as compared to K55 methylation deficient eEF1A (Figure S5C). These results suggest that METTL13-depenent eEF1A K55 dimethylation increases its GTPase activity, which may boost translation elongation and thereby increase protein synthesis.

To analyze the impact of eEF1AK55me2 depletion on mRNA translation we performed polysome profiling experiments on extracts from T3M4 cells ± METTL13 (Gandin et al., 2014). An accumulation of heavy polysomes and a decrease in light polysomes was observed in cells depleted of METTL13 relative to control cells (Figures 5C and S5D). An elevated heavy/light polysome ratio may reflect (i) increase in translation initiation which results in an engagement of a higher number of ribosomes into polysomes thereby suggesting upregulation of protein synthesis or (ii) downregulation of protein synthesis due to the reduction in elongation rates which lead to protracted occupancy and stalling of polysomes on mRNA. Since these scenarios are expected to have opposing effects on mRNA translation rates, we directly measured protein synthesis using surface sensing of translation

(SUnSET) (a method for monitoring global protein synthesis through detection of puromycin-labeled neosynthesized proteins (Schmidt et al., 2009)), in pancreatic (T3M4) and lung (NCI-H2170) cancer cell lines ±METTL13 (Figures 5D-E). In both cancer cell lines, METTL13 depletion decreased global protein synthesis, which was most evident after serum re-feeding of serum-starved cells wherein protein synthesis is acutely stimulated. In contrast, METTL13 depletion had no impact on global protein synthesis in the non-transformed RPE-1 cell line irrespective of conditions (Figure S5E). To avoid potential biases associated with puromycylation approaches, we pulsed cells with the methionine analog L-azidohomoalanine (AHA) (Iwasaki and Ingolia, 2017). When incorporated into newly synthesized proteins, the analog can be detected with streptavidin by first clicking the azide group of AHA to biotin-alkyne. The AHA incorporation assays mirrored results obtained by SUnSET in T3M4 cells (Figure 5F). Moreover, reconstitution of METTL13-depleted T3M4 cells with wild-type METTL13 restored protein synthesis levels to those observed in the control, whereas complementation with catalytic-dead METTL13$_{G58R}$ failed to do so (Figure 5G). Finally, depletion of eEF1A1 and eEF1A2, which as expected resulted in decreased protein synthesis of serum-stimulated cells, was partially rescued by complementation with wild-type eEF1A2, but not with the K55R eEF1A2 mutant (Figure S5F). These data suggest that consistent with its effect on proliferation, eEF1AK55 methylation by METTL13 stimulates protein synthesis in pancreatic cancer cells.

METTL13 ablation inhibits Ras-driven tumorigenesis

METTL13 and eEF1AK55me2 levels negatively correlate with PDAC patient survival, while stimulating processes required for neoplastic growth (i.e. protein synthesis and proliferation). To directly test the role of METTL13 in Ras-driven PDAC, we first generated conditional *Mettl13*$^{loxP/loxP}$ mutant mice, which develop normally, are viable, and fertile (Figure S6A-B). Deletion of *Mettl13* specifically in the pancreas of mice using a pancreas-specific Cre-recombinase expressing strain *Ptf1a*$^{Cre/+}$ (Kawaguchi et al., 2002) resulted in no apparent developmental consequences and no evident physiological defects (data not shown).

Acinar-to-ductal metaplasia (ADM) is an early step in PDAC initiation triggered by KRAS activating mutations (Crawford et al., 2002; Kanda et al., 2012). Using an *ex vivo* 3D culture system in which EGF stimulated RAS activation induces ADM (Guerra et al., 2003; Zhu et al., 2007), as well as *Mettl13* expression (Figure S6B), we found that *Mettl13* deletion inhibited the appearance of duct-like structures (Figure S6C-E). To further investigate the role of METTL13 in KRAS-driven PDAC, *Mettl13* mutant mice were crossed to mice harboring a *loxP*-Stop-*loxP Kras*^{G12D} knock-in allele (*Kras*$^{LSL-G12D/+}$, hereafter *Kras*) (Hingorani et al., 2003), which allows for the controlled induction of oncogenic KRAS and the initiation of cancer. *In vivo,* ADM and PDAC initiation can be triggered in young *Kras* mutant mice by inducing severe acute pancreatitis *via* repeated injections of caerulein (Lee and Bar-Sagi, 2010; Morris et al., 2010) (see schematic Figure 6A). In this system, deletion of *Mettl13,* which led to complete loss of eEF1AK55me2 (Figure 6C and 6E), greatly reduced the appearance of pancreatic intra-epithelial neoplasia (PanIN) brought on by *Kras* activation (Figure 6D), as assessed by histopathological analysis and decreased signals for MUC5 (a marker of PanINs) and Ki67 (proliferation marker) (Figure 6B-E). These data

suggest that METTL13 is required for efficient initiation of pancreatic cancer by oncogenic KRAS.

To study pancreatic tumor development and to perform survival studies, we used the *Ptf1a* $^{+/Cre}$*;Kras*$^{+/LSL-G12D}$*;p53*$^{loxP/loxP}$ (*Kras;p53*) mutant model in which PDAC develops with 100% penetrance 6-8 weeks after birth (Bardeesy et al., 2006). In this aggressive malignancy model, *Mettl13* deletion extended median survival by 60% relative to controls - from 54 days to 86 days (Figure 6F). Accordingly, MRI revealed that tumor volumes in *METTL13* knockouts were roughly reduced by 2/3 as compared to the age-matched control mice (Figure 6G-H) (Mazur et al., 2015). Finally, at autopsy, pancreatic tissue from *Kras;p53* mutant mice is entirely occupied by transformed cells, whereas in *Kras;p53;Mettl13* mutant mice areas of normal pancreatic tissue remain with overall decreased proliferation (Ki67) (Figure 6I-J). Together these data support a key *in vivo* role for METTL13 in oncogenic KRAS-driven pancreatic tumorigenesis.

METTL13 and eEF1A are also potentially involved in lung adenocarcinoma (Figures S4D-F), a cancer in which Ras is frequently activated (Cancer Genome Atlas Research, 2014). We tested METTL13 function in LAC by intratracheal injection of an adenovirus expressing the Cre recombinase (Ad-Cre) in adult *Kras*$^{+/LSL-G12D}$ (*Kras*) and *Kras* $^{+/LSL-G12D}$*;Mettl13*$^{loxP/loxP}$ (*Kras;Mettl13*) mice. As expected *Kras* mutant mice developed widespread adenocarcinoma at 16 weeks after Ad-Cre infection (Jackson et al., 2001; Johnson et al., 2001), which was clearly visible at the whole organ level and by histopathology (Figure 6K). Strikingly, this was paralleled by the upregulation of METTL13 and eEF1AK55me2 (Figure 6K). In contrast *Kras;Mettl13* mutant mice, which are devoid of eEF1AK55me2 (Figure 6K), tumor development was dramatically attenuated based on gross observation, quantification of tumor number and burden, and cell proliferation analysis by phospho-Histone H3 immunostaining (Figure 6K-L). Of note, a substantial fraction of tumors that emerged in the LAC model retained METTL13 expression and eEF1A methylation as assessed by IHC, suggesting incomplete bi-allelic Cre recombination in these clonal growths (Figure S6F) (Jackson et al., 2001; Liu et al., 2010). Together, these *in vivo* data indicate a central role for METTL13 in carcinogenesis of Ras-driven epithelial tumors of the pancreas and lung.

Next, we investigated the role of METTL13-eEF1AK55me2 in human cancers using PDAC and LAC patient-derived xenograft (PDX) models. First, we performed *ex vivo* complementation to knockdown endogenous METTL13 and deplete eEF1AK55me2, and then reconstituted samples with either wild-type or catalytic-dead METTL13 using multiple independent PDXs from both cancers types (Figures 7A-B, S7A-B). The depletion of METTL13 attenuated xenograft tumor growth in both PDAC and LAC models (Figures 7A-B, S7A-B). Complementation with wild-type METTL13, which restored eEF1AK55me2 levels close to the levels of control cells, also reestablished tumor growth (Figures 7A-B, S7A-B). In contrast, reconstitution with METT13$_{G58R}$ did not rescue tumor growth (Figures 7A-B, S7A-B). These data suggest that the pro-tumorigenic functions of METTL13 require its catalytic activity.

A feature of cancers triggered by oncogenes such as KRAS is up-regulation of protein synthesis (Bhat et al., 2015; Robichaud et al., 2018; Truitt and Ruggero, 2016). We postulated that one mechanism by which this may be achieved is through the METTL13-eEF1AK55me2 axis. This led us to speculate that inhibiting METTL13 may cooperate with compounds targeting growth-signaling, which renders malignant cells addicted to increased protein synthesis. To test this idea, a comparative cell-based screen using a library assembled of 285 characterized inhibitors covering ~170 cancer targets (Table S3) was performed to identify drugs that have increased efficacy against T3M4 pancreatic cancer cells in the absence of METTL13. Twelve drugs elicited a 50% increase in synthetic lethality when combined with METTL13 depletion (Table S3); these drugs predominantly inhibit the PI3K-mTOR and MAPK pathways (e.g. Omipalisib, Dactolisib, and Trametinib). Relative to control, treatment of pancreatic (T3M4) and lung (A459) cancer cells with the dual pan-PI3K/mTOR inhibitor Omipalisib or METTL13 depletion had modest effects on proliferation, and the combination of Omipalisib treatment with METTL13 depletion prevented both cell types from growing (Figure 7C-D). To test whether this synergy occurs in an *in vivo* context, PDX tumors ±METTL13 depletion were treated with Omipalisib and tumor growth was monitored (Figure 7E). Notably, PDAC and LAC PDX tumor growth stalled or regressed in size by the combination treatment (Figures 7F-G, S7C-D). Based on our results, we postulate that eEF1AK55 methylation by METTL13 constitutes a hitherto unappreciated mechanism required by neoplasms driven by KRAS pathways to meet their increased protein synthesis requirements (Chio et al., 2016; Martineau et al., 2014; Ruggero et al., 2004). These data also suggest that the METTL13-eEF1AK55me2 axis may constitute a clinically targetable vulnerability of cancers driven by aberrant growth signaling.

DISCUSSION

In a screen of 107 potential KMTs, we identified METTL13 as an active enzyme that specifically di-methylates the elongation factor eEF1A at lysine 55. Based on both depletion and reconstitution experiments in multiple independent cell lines, including primary pancreatic and lung cancer lines, as well as mouse tissue knockouts, we propose that METTL13 is the principal enzyme tasked with generating physiologic eEF1AK55me2. Another functionally important question we address is whether METTL13 has other lysine substrates besides eEF1AK55, particularly in the context of METTL13-associated translation regulation and cancer phenotypes. METTL13 does not methylate histones or any of the proteins stably associated with the 40S and 60S ribosomal subunits or 80S ribosomes. Moreover, eEF1AK55 methylation was the only observed change out of >1000 detected methylation events in cells depleted of METTL13. Consistently with the crucial role of eEF1A1/2 proteins in translation elongation and the pivotal role of protein synthesis in stimulating cell division (Brooks, 1977), we also observed a role for K55 of eEF1A2 in increasing proliferation of pancreatic cancer cells. Together, these findings, in combination with the expression patterns of METTL13 and eEF1AK55me2 in cancer, support our hypothesis that the biological and pathologic functions of METTL13 reported here are mediated through eEF1AK55 methylation. Further support comes from a recently published study that independently identified eEF1AK55 to be specifically methylated by METTL13 (Jakobsson et al., 2018b).

In the methylation of histones, several KMTs are highly selective enzymes with a single physiologic substrate (Carlson and Gozani, 2016); for example, the 7βS KMT hDOT1L recognizes a specific topology (the nucleosome) to methylate a single lysine (H3K79). As with histones, there are several KMTs – including METTL13 – that are devoted to methylating distinct lysines on eEF1A (Hamey and Wilkins, 2018; Jakobsson et al., 2018a). At chromatin, methylation dynamics are regulated not only by KMTs, but also by lysine demethylases and specific methyl-lysine "reader" domains, which together have a major impact in fine-tuning histone functions. We postulate that similar mechanisms are at play in the regulation of translation, and that eEF1A demethylases and readers will soon be identified. Future work may also uncover crosstalk between eEF1AK55 methylation and other eEF1A modifications in the regulation of translation elongation in diverse settings including human disease. Finally, it will also be interesting to explore potential roles for K55me2 in regulating non-canonical eEF1A functions such as RNA export, AKT signaling, and degradation of newly synthesized polypeptides (Abbas et al., 2015; Gandin et al., 2013).

Translation is amongst the most energy consuming processes in cells and dysregulation in translation mechanisms is a common etiologic agent in neoplastic diseases (Bhat et al., 2015; Robichaud et al., 2018; Truitt and Ruggero, 2016). Here we have provided evidence for a model in which METTL13-mediated methylation of eEF1A increases translation elongation and enhances protein synthesis to promote oncogenesis (see Figure S7E). METTL13 and eEF1AK55me2 protein levels are higher in transformed versus non-transformed cells, and higher in malignant Ras-driven pancreatic and lung cancer tissue relative to adjacent normal tissue. Consistently, increased expression of eEF1A1/2 is frequent in malignancies (Lee and Surh, 2009). Deletion of METTL13 profoundly inhibited the ability of oncogenic Ras to drive the development of pancreatic and lung cancers *in vivo* and greatly reduced tumor growth in mice of PDX models from primary human pancreatic and lung tumors. In contrast, METTL13 appears to be dispensable for proliferation of non-transformed cells and normal development of the pancreas. In this regard, the paradigm that translational capacity is in excess in normal tissue but becomes restrictive for tumorigenesis was established in mice haploinsufficient for eIF4E (Truitt et al., 2015). Notably, these mice develop normally, but like METTL13-deleted mice, Ras-driven tumorigenesis is attenuated in the LAC mouse model (Truitt et al., 2015); indeed inhibition of translation initiation with the eIF4A inhibitor SDS-1-021 (Chu et al., 2016) impacted cancer cells with aberrant Ras signaling but not IMR90 cells (Figure S7F-G). Our results raise the possibility that METTL13-eEF1AK55me2 enhancement of translation elongation becomes rate-limiting in growth signal-driven tumors like PDAC and LAC, which could potentially render these lethal cancers vulnerable to METTL13 inhibition. This is consistent with the findings that the eEF2-dependent modulation of translation elongation rates may play a context-dependent role in determining the fate of cancer cells (Faller et al., 2015; Leprivier et al., 2013).

In addition to PDAC and LAC, METTL13 depletion attenuated proliferation in two squamous cell lung cancer cell lines (NCI-H2170 and H520) with activated PI3K, suggesting a relatively broad oncogenic role for METTL13. In a focused cell-based small molecule screen we identified PI3K inhibitors and several other oncogenic growth pathway inhibitors that selectively cooperate with METTL13 depletion to prevent pancreatic and lung

PDX tumor growth. As METTL13 appears to be selectively needed in the transformed cellular state and nonessential in normal tissue, a METTL13 inhibitor, in the context of a combination treatment strategy, may help overcome the narrow therapeutic index of compounds targeting growth signaling (e.g. PI3K) (Infante et al., 2014). In summary, we have identified METTL13 methylation of eEF1AK55 as a mechanism to regulate translation elongation and promote tumorigenesis. These results identify the METTL13-eEF1AK55me2 axis as a vulnerability of growth signaling-driven malignancies and provide a molecular basis for the future development of METTL13 inhibitors for the clinic.

STAR★ METHODS

CONTACT FOR REAGENT AND RESOURCE SHARING

Further information and requests for resources and reagents should be directed to and will be fulfilled by the Lead Contact: Or Gozani (ogozani@stanford.edu).

EXPERIMENTAL MODEL AND SUBJECT DETAILS

Mice—*Ptf1a*$^{+/Cre}$, *Kras*$^{+/LSL-G12D}$, *Trp53*$^{loxP/loxP}$ mice have been described before (Hingorani et al., 2003). Conditional *Mettl13*$^{loxP/loxP}$ gene (NCBI Reference Sequence: NM_144877.1) knockout mice were generated in this study. Briefly, to engineer the targeting vector, homology arms and exon 3 (conditional knockout region) was generated by PCR using BAC clone RP23-270A15 and RP24-316J6 from the C57BL/6J library as template. The targeting vector includes the self-excising Neo cassette flanked by Rox sites and exon 3 sequence were flanked by LoxP sites. DTA cassette (Diphtheria Toxin A) was used for negative selection. The linearized vector was subsequently delivered to ES cells (C57BL/6) *via* electroporation, followed by drug selection, PCR screening, and Southern Blot confirmation. Correctly targeted ES clones were selected for blastocyst microinjection, followed by founder mice production. Founders were confirmed as germline-transmitted *via* crossbreeding with wild-type animals. In conjunction with germ line transmission of the mutant allele the self-excising Neo cassette was deleted. Mice were in a mixed C57BL/6;129/Sv background, and we systematically used littermates as controls in all the experiments. Immunocompromised NSG mice (*NOD.SCID-IL2Rg*$^{-/-}$) were utilized for transplantation studies. All experiments were performed on balanced cohorts of male and female mice as our initial data did not indicate significant differences in disease progression or response to treatment between females or males. All animals were numbered and experiments were conducted in a blinded fashion. After data collection, genotypes were revealed and animals assigned to groups for analysis. For treatment experiments mice were randomized. None of the mice with the appropriate genotype were excluded from this study or used in any other experiments. Mice had not undergone prior treatment or procedures. Husbandry and housing conditions: All mice were fed a standard chow diet *ad libitum* and housed in pathogen-free facility with standard controlled temperature, humidity, and light-dark cycle (12h) conditions with no more than 5 mice per cage under the supervision of veterinarians, in an AALAC-accredited animal facility at the University of Texas M.D. Anderson Cancer Center. All animal procedures were reviewed and approved by the MDACC Institutional Animal Care and Use Committee (IACUC 00001636, PI: Mazur).

Cell Lines—293T (female, embryonic kidney) cells were grown in DMEM medium supplemented with 10% fetal calf serum. U2OS (human bone osteosarcoma) cells were cultured in McCoy's 5a medium supplemented with 10% fetal bovine serum and 100 U/mL penicillin/streptomycin. Colo-357 (female, 77 years old, pancreatic cancer), L3.3 (female, 77 years old, pancreatic cancer), PaTu8902 (female, 44 years old, pancreatic cancer), and T3M4 (male, age not reported, pancreatic cancer) and HT1080 (male, 35 years old, fibrosarcoma) cells were cultured in DMEM supplemented with 10% fetal bovine serum, glutamine, and 100 U/mL penicillin/streptomycin. NCI-H2170 (male, age not reported, lung cancer) and NCI-H520 (male, age not reported, lung cancer) cells were cultured in RPMI 1640 medium supplemented with 10% fetal bovine serum and 100 U/mL penicillin/ streptomycin. RPE-1 cells (human epithelial cells immortalized with hTERT) were from ATCC and cultured in DMEM:F12 medium supplemented with 10% fetal bovine serum, 100 U/mL penicillin/streptomycin, and 0.01mg/mL hygromycin B. IMR-90 (female, 16 weeks gestation, normal lung fibroblast) were from ATCC and cultured in EMEM supplemented with 10% fetal bovine serum and 100 U/mL penicillin/streptomycin. All cells were cultured at 37°C in a humidified incubator with 5% CO_2. Cell lines were authenticated by short tandem repeat profiling and tested negative for mycoplasma (DDC Medical). Serum stimulation was performed after serum-starving overnight using regular 10% fetal bovine serum. For quantitative proteomics, wild-type and METTL13-depleted T3M4 cells were grown in SILAC media containing light or heavy amino acids (^{13}C ^{15}N -L-lysine/^{13}C ^{15}N - L-arginine, see Key Resources Table).

Human Tumor Samples—Surgically resected tumor specimens were obtained from patients with histologically confirmed pancreatic cancer and non-small cell lung cancer blinded for age and gender. All surgically resected tumors were collected after written patient consent and in accordance with the institutional review board-approved protocols of the University of Texas M.D. Anderson Cancer Center (LAB07-0854, LAB10-0704). Information on gender and age were not associated with tumor samples and hence blinded.

METHOD DETAILS

Pancreatic Cancer Mouse Models—For pancreatic cancer initiation studies acute pancreatitis was induced at 6 to 8 weeks of age in $Ptf1a^{+/Cre};Kras^{+/LSL-G12D}$ ($Kras$) and $Ptf1a^{+/Cre}; Kras^{+/LSL-G12D}; Mettl13^{loxP/loxP}$ ($Kras;Mettl13$) mice by administration of 8 hourly intraperitoneal (IP) injections of caerulein (100 μg/kg body weight) over 2 consecutive days as described previously (Mazur et al., 2014). Pancreatic lesions were analyzed 10 d after the last injection. For survival studies, we used $Ptf1a^{+/Cre};Kras^{+/LSL-G12D}; Trp53^{loxP/loxP}$ ($Kras;p53$) and $Ptf1a^{+/Cre};Kras^{+/LSL-G12D};Trp53^{loxP/loxP}; Mettl13^{loxP/loxP}$ ($Kras;p53;Mettl13$) mice, which develop aggressive disease. Mice were followed for signs of disease progression. At the end of the experiment, tumors were processed for biochemical, histological and immunohistochemical analysis. Histopathological analysis was conducted on de-identified slides based on the classification consensus.

Lung Adenocarcinoma Mouse Models—To generate tumors sporadically in the lungs of $Kras^{+/LSL-G12D}$ and $Kras^{+/LSL-G12D}; Mettl13^{loxP/loxP}$ mutant mice, we used replication-

deficient adenoviruses expressing Cre-recombinase (Ad-Cre) to deliver transient Cre recombinase expression to infected cells of the lung, as previously described (Mazur et al., 2014). Briefly, 8 to 10-week old mice were anesthetized by continuous gaseous infusion of 2% isoflurane for at least 10 min using a veterinary anesthesia system (D19 Vaporizer, Vetland Medical). Ad-Cre was delivered to the lungs by intratracheal intubation. Prior to administration, Ad-Cre was precipitated with calcium phosphate to improve the delivery of Cre by increasing the efficiency of viral infection of the lung epithelium. Mice were treated with one dose of 5×10^6 PFU of Ad-Cre (Baylor College of Medicine, Viral Vector Production Core). Mice were analyzed for tumor formation and progression at 16 weeks after infection.

Magnetic Resonance Imaging—Magnetic Resonance Imaging (MRI) experiments were performed on *Kras;p53* and *Kras;p53;Mettl13* mutant mice at an age of 7 weeks. Before imaging, mice were anesthetized by continuous gaseous infusion of 2% isoflurane for at least 10 min using a veterinary anesthesia system (D19 Vaporizer, Vetland Medical). During imaging, the dose was kept at 2% isoflurane, animal temperature was maintained and continuously monitored, respiratory and ECG monitoring were performed using an MRI-compatible physiological monitoring system (Small Animal Instruments, Inc) and eyes were protected with an eye ointment. MRI was performed using the Biospec USR70/30 (Bruker Biospin MRI, Billerica, MA) a small animal experimental MR imaging system based on an actively-shielded 7 T magnet with a 30 cm bore and cryo-refrigeration. The system is equipped with 6 cm inner-diameter gradients that deliver a maximum gradient field of 950 mT m–1. A 3.5 cm inner-diameter linear birdcage coil transmits and receives the MR signal. For image acquisition, T2-weighted, respiratory gated, multi-slice imaging will be performed with respiration held to under 25 breaths per minute to minimize motion artefacts in the abdomen. The rapid acquisition with relaxation enhancement (RARE) T2-weighted pulse sequence was modified to include an effective Te (time of echo) of 38 ms, echo train length 9.5 ms, and number of averages equal to 4 in both the coronal and axial planes with a total TR (time repetition) of 2000 ms. A three-orientation (axial, sagittal, and coronal) scout image using a fast, low-angle single shot sequence was obtained to localize the mouse pancreas. Between 18 and 20 coronal and axial slices were acquired per mouse with a slice thickness of 0.7 mm and slice spacing of 1 mm to cover the entire pancreas. In plane, pixel sizes of 0.156 mm × 0.156 mm with a matrix size of 256 × 192 and field of view (FOV) of 40 mm × 30 mm was chosen to minimize in plane partial volume effects, maintain a FOV sufficient to cover the abdomen, while also providing sufficient throughput for the experiment. MR images were analyzed using an open source Horos processing software. Pancreas tumor burden was measured by tracing the outer border of the region of suspected lesions on each slice after image intensities were normalized. Analysis was conducted on de-identified images. Tumor volume (V) was assessed, using three-dimensional volumetric measurements according to the modified Simpson rule. In all contiguous transverse images, the area of tumor (A) in each slice was multiplied by the slice profile (0.7 mm slice thickness plus 1 mm intersection gap), and total tumor volume was automatically calculated by summation of the adjacent volume according to the formula:

$$V = T_s \times \left(\sum_{i=1}^{n} A_i \right)$$

where T_s is the thickness of each slice, i is the individual slice number and n is the total number of slices.

Histology and Immunohistochemistry—Tissue specimens were fixed in 4% buffered formalin for 24 hours and stored in 70% ethanol until paraffin embedding. 3-μm sections were stained with hematoxylin and eosin (HE) or used for immunohistochemical studies. Human tissue sections were collected in accordance with the institutional review board-approved protocols of the University of Texas M.D. Anderson Cancer Center (LAB05-0854). Immunohistochemistry (IHC) was performed on formalin-fixed, paraffin embedded mouse and human tissue sections using a biotin-avidin method as described before (Mazur et al., 2014). The following antibodies were used (at the indicated dilutions): cleaved caspase 3 (1:200), Ki67 (1:1,000), MUC5AC (1:500), METTL13 (1:100) and eEF1AK55me2 (1:500). Sections were developed with DAB and counterstained with hematoxylin. Pictures were taken using a Leica microscope equipped with the LAX software. Analysis of the tumor area and IHC analysis was done using ImageJ software by measuring pixel units. Quantification of chromogen intensity was performed by measuring the reciprocal intensity of the chromogen stain. Briefly, standard RGB color images acquired from bright field microscopy have a maximum intensity of value 250 (represented by white, unstained areas) as measured by the standard intensity function in the open source Fiji software (ImageJ). We subtracted the intensity of a stained tissue sample from 250, thereby deriving a reciprocal intensity that is directly proportional to the amount of chromogen present.

Preparation of Pancreatic Epithelial Explants Culture—Pancreatic epithelial explants from 6-week old wild-type mice were established by modification of previously published protocols (Mazur et al., 2014). In brief, the whole pancreas was harvested and treated twice with 1.2 mg/ml Collagenase VIII. Following multiple wash steps with McCoy's medium containing soybean trypsin inhibitor (SBTI, 0.2 mg/ml), digested samples were filtered through a 100 μm filter, resuspended in culture medium (Waymouth's MB 752/1 supplemented with 0.1% BSA, 0.2 mg/ml SBTI; 50 μg/ml bovine pituitary extract, 10 μg/ml Insulin, 5 μg/ml transferrin, 6.7 ng/ml selenium in 30% fetal bovine serum) and allowed to recover for 1h at 37°C. Thereafter, cells were pelleted and resuspended in culture medium supplemented with penicillin G (1000 U/ml), streptomycin (100 μg/ml), amphotericin B, 0.1% fetal bovine serum, and an equal volume of rat tail collagen and immediately plated on plates pre-coated with 2.5 mg/ml of rat tail collagen type I. In stimulation experiments, recombinant mouse EGF was added to a final concentration of 25 ng/ml. For quantification, acinar explants were seeded in triplicate. Cell clusters were counted from at least 3 optical fields/well and reported as a percentage of acinar clusters and duct-like spheres. The quantification was performed in two independent experiments; the number of mice is reported in the main text.

Meta-analysis of Gene Expression—Meta-analysis of public PDAC and NSCLC data sets. We downloaded raw data for gene expression studies (7 pancreatic cancer, 6 NSCLC) from the NCBI GEO and EBI ArrayExpress. After re-annotating the probes, each data set was normalized separately using gcRMA. We applied two meta-analysis approaches to the normalized data. Briefly, the first approach combines effect sizes from each data set into a meta-effect size to estimate the amount of change in expression across all data sets. For each gene in each data set, an effect size was computed using Hedges' adjusted g. If multiple probes mapped to a gene, the effect size for each gene was summarized using the fixed effect inverse-variance model. We combined study-specific effect sizes to obtain the pooled effect size and its standard error using the random effects inverse-variance technique. We computed z-statistics as a ratio of the pooled effect size to its standard error for each gene and compared the result to a standard normal distribution to obtain a nominal *P*-value. *P*-values were corrected for multiple hypotheses testing using false discovery rate (FDR). We used a second non-parametric meta-analysis that combines *P*-values from individual experiments to identify genes with a large effect size in all data sets. Briefly, we calculated a t-statistic for each gene in each study. After computing one-tail *P*-values for each gene, they were corrected for multiple hypotheses using FDR. Next, we used Fisher's sum of logs method, which sums the logarithm of corrected *P*-values across all data sets for each gene and compares the sum against a chi-square distribution with 2k degrees of freedom, where k is the number of data sets used in the analysis.

Patient-derived Cancer Xenografts—Surgically resected tumor specimens were obtained from patients with histologically confirmed pancreatic cancer and non-small cell lung cancer blinded for age and gender. All surgically resected tumors were collected after written patient consent and in accordance with the institutional review board-approved protocols of the University of Texas M.D. Anderson Cancer Center (LAB07-0854, LAB10-0704). Patient-derived xenograft tumors were generated by transplanting small tumor fragments isolated directly from surgical specimens subcutaneously into mice. In each case we first propagated the sample in NSG mice. For reconstitution assays, collected PDX tumors were minced using a razor blade and digested in collagenase digestion buffer at 37°C for 1 hour. Cells were passed through 100 μm and 40 μm cell strainers and centrifuged for 1200 rpm for 8 min. Cells were incubated in RBC lysis buffer for 2 min and then resuspended in 6 mL of media and spun through 0.5mL of serum layered on the bottom of the tube to remove cellular debris. Contaminating human or mouse hematopoietic and endothelial cells (CD45, Ter119, CD31) are depleted using biotin conjugated anti-mouse CD45, CD31 and Ter119 antibodies and separated on a MACS LS column using anti biotin microbeads. The isolated cells are transiently cultured on several matrigel coated plates and infected with lentivirus carrying sgRNA Mettl13 (shMettl13) and cDNA of METTL13 WT, METTL13 catalytic dead mutant and briefly selected using appropriate antibiotics. Then cells were collected, mixed with matrigel (1:1) and transplanted to the flanks of NSG mice. When tumors became palpable, they were calipered every 3 days to monitor growth kinetics. Tumor volume was calculated using the formula: Volume = $(width)^2 \times length / 2$ where *length* represents the largest tumor diameter and *width* represents the perpendicular tumor diameter.

Transfection and Viral Transduction—Transient expression was performed using TransIT-293 (Mirus Bio) following the manufacturer's protocol. For CRISPR/Cas9 knockouts, virus particles were produced by co-transfection of 293T cells with the lentiCRISPR v2 /hygro construct expressing indicated sgRNAs, pCMV-VSV-G and pCMV-dR8.2 dvpr in a ratio of 5:2:3 by mass. 48 hours after transfection, target cells were transduced with 0.45 μm filtered viral supernatant and 4 μg/mL polybrene. Cells were selected 24h after media replacement with 12.5 μg/mL puromycin for RPE-1 or 250 μg/mL hygromycin B for other cell lines. For METTL13 reconstitution, cells were transduced with retroviral pBABE or pWZL constructs using pUMVC and pCMV-VSV-G in a ratio of 2:1:1 by mass. The subsequent selection was carried out with 800 μg/mL G-418 for NCI-H2170, 2 mg/mL G-418 for T3M4, or 10 μg/mL blasticidin for 293T cells. For eEF1A2 reconstitution, T3M4 cells were transduced with pLenti6.2 plasmid, pCMV-dR8.2 dvpr and pCMV-VSV-G in a ratio of 5:3:2 by mass and selected with 20 μg/mL blasticidin.

Plasmids—Protein sequences were METTL13 (accession no. NP_057019.3), eEF1A1 (accession no. NP_001393.1), and eEF1A2 (accession no. NP_001949.1). Bacterial expression plasmids were created using pGEX-6P-1. Transient mammalian expression was conducted using pcDNA3.1(+). lentiCRISPRv2 was used for CRISPR/Cas9 knockouts in RPE-1 cells, while lentiCRISPRv2 hygro were used in all other cell lines. For stable expression in mammalian cells, METTL13 was cloned into pBABE-neo and pWZL Blast GFP. eEF1A2 was originally cloned into pENTR3C and then recombined into pLenti6.2 V5-DEST. The inserts were amplified by PCR using specific clones from the human ORFeome library as templates. Single point mutations of METTL13 and eEF1A2 were generated by site-directed mutagenesis.

CRISPR/Cas9 Knockout Library Screen—107 known and candidate lysine methyltransferases (KMTs) were identified based on literatrure analyses (e.g. (Clarke, 2013)). The top three sgRNAs targeting each putative KMT were taken from a previously published genome-wide human sgRNA library (Morgens et al., 2017) (Table S1). The control sgRNA, which shows no effect on growth in multiple cell lines, was designed to be at least 2 bases mismatched to anything in the human genome. A total of 322 KMT sgRNAs were cloned into the lentiCRISPR v2 vector. Lentivirus particles were produced as described above. U2OS cells in 6-well plates were infected with virus in 4 μg/mL polybrene for 2 days, then expanded into 10 cm plates for 3 days in puromycin at 2 μg/mL. Lysate from each plate was collected in 1 mL RIPA buffer (10 mM Tris-HCl pH 8, 150 mM NaCl, 1 mM EDTA, 0.5 mM EGTA, 1% Triton, 0.1% SDS) supplemented with protease inhibitor cocktail. For Western analysis, 40 μL of cell lysates were mixed with 10 μL of 5× SDS loading buffer and boiled for 5 min. 20 μL was resolved by SDS-PAGE, transferred to a PVDF membrane, and probed with the anti-eEF1AK55me2 antibody for screening. Tubulin was used as a loading control.

Immunoblot Analysis and Immunoprecipitation—For Western blot analysis, cells were lysed in RIPA buffer with 1 mM PMSF and protease inhibitor cocktail. Protein concentration was determined using the Pierce Coomassie Plus Assay. Protein samples were resolved by SDS-PAGE and transferred to a PVDF membrane (0.45 μm). Dot blot analysis

was performed by directly loading 1 μL of the indicated amounts of biotinylated peptides onto a PVDF membrane (0.2 μm). The following antibodies were used (at the indicated dilutions): eEF1AK55me1 (1:3,000), eEF1AK55me2 (1:10,000), eEF1AK55me3 (1:5,000), eEF1A (1:5,000), beta-tubulin (1:5,000), puromycin (1:2,000), METTL13 (1:2,000), peroxidase-conjugated streptavidin (1:10,000), eIF3A (1:5,000), RPS6 (1:2,000), RPL6 (1:3,000), eEF1A2 (1:2,000). All secondary antibodies were used at 1:10,000 dilution. Protein bands were visualized using Amersham ECL or Amersham ECL Prime Western Blotting Detection Reagent.

For immunoprecipitation of endogenous eEF1A, equal amounts of whole cell extracts (WCEs) were incubated with anti-eEF1A at 4°C for overnight and then with protein G magnetic beads at 4°C for 2 hours. The beads were washed with cell lysis buffer at 4°C three times, boiled in Laemmli buffer, and then frozen until processed for MS analysis as described below.

Expression and Purification of Recombinant Proteins—GST fusion proteins were expressed in BL21 *Escherichia coli* by overnight culture at 2°C in LB medium (10 g/L tryptone, 5 g/L yeast extract, and 10 g/L NaCl) supplemented with 0.1 mM IPTG (isopropyl 1-thio- β-D-galactopyranoside, Sigma), purified using Glutathione Sepharose 4B (GE Healthcare) and eluted in 10 mM reduced glutathione (Sigma). Protein concentrations were measured using Pierce Coomassie Plus Assay. DTT was added to the protein solution at a final concentration of 20 mM. Recombinant human core histones were expressed and purified by ion-exchange chromatography. The histones were combined in equimolar ratio under denaturing conditions and dialyzed against high salt buffer to assemble octamers. Octamers were purified by gel filtration chromatography. Nucleosomes were subsequently assembled with the optimized 601 DNA sequence that was amplified with a 5' biotinylated primer.

For purification of Flag-tagged eEF1A1, eEF1A1 bearing a C-terminal Flag tag was expressed by transient transfection in wild-type or METLL13-depleted 293T cells that were reconstituted with METTL13$_{WT}$ or METTL13$_{G58R}$, respectively. After 48h transfection, eEF1A was isolated from whole cell extracts using anti-Flag M2 affinity gel (Sigma) according to the instructions of the manufacturer and eluted with 3×Flag peptides (Sigma). The resulting purified eEF1A1 was immediately used for enzymatic reactions.

Structural Modeling of METTL13 (1-400)—Structural modeling of the first 400 residues of METTL13 (METTL13 1-400) was performed using the I-TASSER software package. Based on the amino acid sequence of METTL13$_{1-400}$, the program identified structural templates from Protein Data Bank (https://www.rcsb.org/), which were then subject to template-based fragment assembly simulations to generate the structural model. The relative orientation of the two subdomains of METTL13$_{1-400}$, MTase and SBD, was manually arranged in a similar manner as that of the corresponding domains of PrmA (Demirci et al., 2007).

Polysome Profiling—Wild-type or METTL13-depleted T3M4 cells were seeded into six 15-cm Petri dishes (~10×10^6 cells per dish) 24 hours prior to serum starvation for 16h

followed by replacement with fresh medium for 2h. Cells were treated with 100 μg/mL cycloheximide and incubated for 2 min at 37°C. Cells were washed and scraped in cold PBS containing 100 μg/mL cycloheximide, pelleted and lysed in lysis buffer (5 mM Tris pH7.4, 2.5 mM MgCl2, 1.5 mM KCl, 100 μg/mL cycloheximide, 2 μM DTT, 0.5% Triton, 0.5% Na-DOC, 100 U/mL SUPERase In RNase inhibitor and protease inhibitors). Lysates were cleared for 10 min at 14,000 rpm at 4°C. RNA contents were determined by Nanodrop and 500 μg of RNA were loaded on 10% to 50% sucrose gradients made in 15 mM Tris pH7.4, 15 mM MgCl$_2$, 150 mM NaCl and prepared using a BioComp Gradient Station. Gradients were spun for 2 hours in a TH-641 rotor (Sorvall) at 40,000 rpm and 4°C. Gradients were analyzed (260 nm) and fractions collected with a BioComp Gradient Station.

Methylation and GTPase Assays—_In vitro_ methylation assays were performed similar to as descrbied in (Mazur et al., 2014) by combining 3 μg of recombinant proteins or 1 μg of peptides and equal amounts of recombinant enzymes in a methyltransferase buffer (50 mM Tris pH 8.0, 20 mM KCl, 5 mM MgCl$_2$, and 10% glycerol) supplemented with 1 mM S-adenosyl-methionine (SAM, New England Biolabs) or deuterated AdoMet (C/D/N Isotopes) or 2 μCi of tritiated AdoMet (American Radiolabeled Chemicals). The reaction mixtures were incubated overnight at 30°C. Reactions were resolved by SDS-PAGE, followed by autoradiography, Coomassie stain or mass spectrometry analysis.

For _in vitro_ methylation assay on ribosomes, 40S and 60S ribosomal subunits and 80S ribosomes were isolated from cytoplasmic extract of T3M4 cells as described in **Polysome Profiling**. The eluting fractions were dialyzed twice in 2 L of 100 mM Tris, pH 8.0 (MCWO 3500) and then concentrated (MWCO 3000) by centrifugation at 14,000 × g. Methylation reactions were carried out in the methyltransferase buffer containing 3 μg of recombinant METTL13 (amino acids 1-498), 17.5 μL of concentrated ribosomes, and 1 mM _S_-adenosyl-methionine or 2 μCi of tritiated AdoMet at 30°C for overnight. The reactions were resolved by SDS-PAGE, followed by autoradiography, Coomassie stain or Western blot analysis.

GTPase assays were performed in triplicate using ATPase/GTPase Activity Assay Kit (Sigma) following the manufacturer's protocol. Briefly, 3 μg of Flag-tagged eEF1A1K55me0/2 purified from 293T cells (as described above) were incubated with increasing amounts of GTP in 30 μL of the reaction buffer provided by the kit at 37μC for 3 hours. The reactions were terminated by adding 200 μL of the kit reagent and incubating for an additional 30 min at room temperature. For GTPase activation by aminoacyl-tRNA (aa-tRNA), the GTPase assays were performed using 3 μg of Flag-tagged eEF1A1K55me0/2, 500 μM GTP, 100 ng/pL total aa-tRNAs and 25-30 units RNasin ribonuclease inhibitors (Promega) in 30 μL of the reaction buffer. Isolation of total aa-tRNAs from 293T cells was performed at 4°C using phenol/chloroform extraction under acidic conditions. Formation of hydrolyzed free phosphate was measured at a wavelength of 620 nm, and absorbance was compared with a standard curve. The readings of background blank and negative control reactions were subtracted from the sample readings. The kinetic parameters were evaluated by fitting the data to the Michaelis-Menten equation in Origin Pro 8.

Mass Spectrometry (MS) of eEF1AK55 Methylation—Recombinant and immunoprecipitated eEF1A were separated by SDS-PAGE and stained using InstantBlue

Protein Stain (Expedeon). Bands were cut and destained in 50% acetonitrile (ACN), 50% ammonium bicarbonate (NH_4HCO_3, 50mM) for 10 min twice. Gel pieces were incubated in 50 mM NH_4HCO_3 containing 10 mM DTT at 60'C for 30 min, followed by treatment with 25 mM iodoacetamide in 50 mM NH_4HCO_3 at room temperature for 45 min. In-gel digestion was performed using 100 ng/μL Glu-C in 50 mM phosphate buffer (pH 7.8) at 37'C or 10 ng/μL trypsin in 50 mM NH_4HCO_3 at room temperature for overnight. Two consecutive peptide extractions were processed with 5% formic acid, 49% water, and 50% ACN. The resulting peptides were dried by speedvac, desalted using C18 StageTips (Thermo Fisher Scientific), and analyzed on an Orbitrap Elite mass spectrometer. Methylation states of eEF1AK55 were manually inspected. Selected ion chromatograms for peptides spanning eEF1AK55 were extracted using Xcalibur Qual Browser (Thermo). The settings were as follows:

Peptide 49-61, m/z 501.255 (me0), 505.927 (me1), 510.599 (me2) and 515.271 (me3), 10 p.p.m

Peptide 49-61 (deuterated K55me), m/z 501.255 (me0), 506.933 (me1), 512.6115 (me2) and 518.290 (me3), 10 p.p.m

Peptide 52-62, m/z 664.356 (me1), 671.364 (me2) and 678.372 (me3), 10 p.p.m

Peptide 52-62 (deuterated K55me), m/z 665.865 (me1), 674.382 (me2) and 682.900 (me3), 10 p.p.m

Proteome-wide Labeling and Analysis of METTL13 Substrates—Wild-type and METTL13-depleted T3M4 cells were grown in SILAC media containing either normal amino acids ('light') or modified amino acids ('heavy") for two weeks and lysed in RIPA buffer with 1 mM PMSF and protease inhibitor cocktail. A 2-way experiment was performed – the 'forward' condition combining light WCE + METTL13 with heavy WCE - METTL13 and the 'reverse' condition combining heavy WCE + METTL13 with light WCE - METTL13 at a ratio of 1:1 by mass. 10 μg of the lysates of each pair were resolved by SDS-PAGE and stained using a SilverQuest Silver Staining Kit. Gel pieces were treated with DTT and iodoacetamide as described above. In-gel digestion was performed using 25 ng/μL trypsin followed by purification using C18 stage tips. To best extract the methylated peptides from the entire proteome, the resulting digestion products were analyzed on an Orbitrap Elite mass spectrometer and an Orbitrap Fusion mass spectrometer (Thermo Scientific). Data obtained from the two instruments were combined and processed using MaxQuant version 1.3.0.5 (Cox and Mann, 2008) and allowing as variable modifications – methionine oxidation; mono- and di-methylation of arginine; and mono-, di- and tri-methylation of lysine.

Cell Assays—For cell proliferation assays, cells were seeded at 2×10^5 cells/mL in triplicate in 6-well plates. Cell counts were acquired by Countess II FL Automated Cell Counter (Thermo Fisher Scientific) at indicated days for 8-10 days. After each counting, the cells were maintained at a density between $2\text{-}4 \times 10^5$ cells/mL. Trypan blue was used to stain non-viable cells. Cell numbers were expressed relative to 1×10^5 cells/mL.

Bromodeoxyuridine (BrdU) incorporation assay were conducted fusing Cell Proliferation ELISA BrdU Kit. Cells were seeded in 96-well plates (1,000 cells/well for HT1080, PaTu8902; 2,000 cells/well for T3M4 and colo-357; and 4000 cells for IMR90) and treated with drug concentrations as indicated in the text or with a vehicle for 72h. Absorbance at 370 nm (corrected for absorbance at the reference wavelength of 492 nm) was measured using a microplate reader (Benchmark Plus microplate reader; Bio-Rad) according to a manufacturer's instructions. Tests were performed in two biological replicates, each carried out in a triplicate. BrdU incorporation is expressed as a fraction of vehicle (DMSO) treated control. For viable cell counting, 1×10^5 HT1080, PaTu8902, T3M4 and colo-357 cells and 2×10^5 IMR90 cells were seeded in 6-well plates and treated with drug concentrations as indicated in the text or with a vehicle for 72h. Non-viable cells were excluded using Trypan blue staining. Tests were performed in two biological replicates, each carried out in a triplicate. Viable cell count is expressed as a fraction of vehicle (DMSO) treated control. Proliferation curves were generated and fitted using GraphPad [using log(inhibitor) vs response – Variable slope (four parameters)].

Translation Assays—For SUnSET assays (Schmidt et al., 2009), wild-type or METTL13-depleted T3M4 and NCI-H2170 cells were seeded at $2\text{-}4 \times 10^5$ cells/mL in 6-well plates 24 hours prior to serum starvation. For serum stimulation, cells were maintained in regular media containing 10% fetal bovine serum for an optimized period (2 hours for T3M4 and 1 h for NCI-H2170). Puromycin pulses were performed by incubating the cells with 10 μg/mL puromycin for 15 min at 37°C. Cells were then washed with cold PBS and lysed in RIPA buffer supplemented with 1 mM PMSF and protease inhibitor mixture. 5-10 μg of the whole cell lysate were assayed by Western blot analysis using the anti-puromycin antibody.

For labeling newly synthesized proteins, T3M4 cells were maintained in DMEM free of cysteine and methionine for 1h, then grown in DMEM containing 100 μg/mL methionine or AHA (l-azidohomoalanine) for 2 hours. T3M4 cells under serum starvation were cultured in DMEM free of cysteine and methionine for 1h, then grown for 2h in DMEM containing 10% fetal bovine serum and 100 μg/mL methionine or AHA. Cells were then harvested, washed with PBS on ice and lysed in RIPA buffer. Click reactions were performed using Click Chemistry Reaction Buffer Kit (Click Chemistry Tools) following the manufacturer's protocol. Briefly, 50-100 μg of whole cell lysates were incubated with 40 μM Biotin-PEG4-Alkyne for 30 min. The proteins were extracted with methanol and chloroform and 1-5 μg were assayed by Western blot analysis using streptavidin-conjugated horseradish peroxidase.

QUANTIFICATION AND STATISTICAL ANALYSIS

Please refer to the Figure Legends or the Experimental Details for description of sample size (*n*) and statistical details. All values for *n* are for individual mice or individual sample. Sample sizes were chosen based on previous experience with given experiments. Cell culture assays have been performed in triplicates and in two independent experiments, unless stated otherwise. Data are expressed as mean ± SEM. Differences were analyzed by Spearman's rank correlation, log-rank, two-tailed Student's t test, Mann-Whitney U test,

one-way ANOVA (using Bonferroni post test), one-sample t test or c2-test using Prism 7 (GraphPad), *P*-values 0.05 were considered significant.

Supplementary Material

Refer to Web version on PubMed Central for supplementary material.

ACKNOWLEDGEMENTS

REFERENCES:

Abbas W, Kumar A, and Herbein G (2015). The eEF1A Proteins: At the Crossroads of Oncogenesis, Apoptosis, and Viral Infections. Front Oncol 5, 75. [PubMed: 25905039]

Bardeesy N, Aguirre AJ, Chu GC, Cheng KH, Lopez LV, Hezel AF, Feng B, Brennan C, Weissleder R, Mahmood U, et al. (2006). Both p16(Ink4a) and the p19(Arf)-p53 pathway constrain progression of pancreatic adenocarcinoma in the mouse. Proceedings of the National Academy of Sciences of the United States of America 103, 5947–5952. [PubMed: 16585505]

Bhat M, Robichaud N, Hulea L, Sonenberg N, Pelletier J, and Topisirovic I (2015). Targeting the translation machinery in cancer. Nat Rev Drug Discov 14, 261–278. [PubMed: 25743081]

Brooks RF (1977). Continuous protein synthesis is required to maintain the probability of entry into S phase. Cell 12, 311–317. [PubMed: 902318]

Cancer Genome Atlas Research, N. (2014). Comprehensive molecular profiling of lung adenocarcinoma. Nature 511, 543–550. [PubMed: 25079552]

Carlson SM, and Gozani O (2016). Nonhistone Lysine Methylation in the Regulation of Cancer Pathways. Cold Spring Harb Perspect Med 6.

Cavallius J, and Merrick WC (1998). Site-directed mutagenesis of yeast eEF1A. Viable mutants with altered nucleotide specificity. J Biol Chem 273, 28752–28758. [PubMed: 9786872]

Chi P, Allis CD, and Wang GG (2010). Covalent histone modifications--miswritten, misinterpreted and mis-erased in human cancers. Nat Rev Cancer 10, 457–469. [PubMed: 20574448]

Chio IIC, Jafarnejad SM, Ponz-Sarvise M, Park Y, Rivera K, Palm W, Wilson J, Sangar V, Hao Y, Ohlund D, et al. (2016). NRF2 Promotes Tumor Maintenance by Modulating mRNA Translation in Pancreatic Cancer. Cell 166, 963–976. [PubMed: 27477511]

Chu J, Cencic R, Wang W, Porco JA Jr., and Pelletier J (2016). Translation Inhibition by Rocaglates Is Independent of eIF4E Phosphorylation Status. Mol Cancer Ther 15, 136–141. [PubMed: 26586722]

Clarke SG (2013). Protein methylation at the surface and buried deep: thinking outside the histone box. Trends Biochem Sci 38, 243–252. [PubMed: 23490039]

Cox J, and Mann M (2008). MaxQuant enables high peptide identification rates, individualized p.p.b.-range mass accuracies and proteome-wide protein quantification. Nat Biotechnol 26, 1367–1372. [PubMed: 19029910]

Crawford HC, Scoggins CR, Washington MK, Matrisian LM, and Leach SD (2002). Matrix metalloproteinase-7 is expressed by pancreatic cancer precursors and regulates acinar-to-ductal metaplasia in exocrine pancreas. J Clin Invest 109, 1437–1444. [PubMed: 12045257]

Demirci H, Gregory ST, Dahlberg AE, and Jogl G (2007). Recognition of ribosomal protein L11 by the protein trimethyltransferase PrmA. EMBO J 26, 567–577. [PubMed: 17215866]

Faller WJ, Jackson TJ, Knight JR, Ridgway RA, Jamieson T, Karim SA, Jones C, Radulescu S, Huels DJ, Myant KB, et al. (2015). mTORC1-mediated translational elongation limits intestinal tumour initiation and growth. Nature 517, 497–500. [PubMed: 25383520]

Gandin V, Gutierrez GJ, Brill LM, Varsano T, Feng Y, Aza-Blanc P, Au Q, McLaughlan S, Ferreira TA, Alain T, et al. (2013). Degradation of newly synthesized polypeptides by ribosome-associated RACK1/c-Jun N-terminal kinase/eukaryotic elongation factor 1A2 complex. Molecular and cellular biology 33, 2510–2526. [PubMed: 23608534]

Gandin V, Sikstrom K, Alain T, Morita M, McLaughlan S, Larsson O, and Topisirovic I (2014). Polysome fractionation and analysis of mammalian translatomes on a genome-wide scale. J Vis Exp.

Guerra C, Mijimolle N, Dhawahir A, Dubus P, Barradas M, Serrano M, Campuzano V, and Barbacid M (2003). Tumor induction by an endogenous K-ras oncogene is highly dependent on cellular context. Cancer Cell 4, 111–120. [PubMed: 12957286]

Hamey JJ, and Wilkins MR (2018). Methylation of Elongation Factor 1A: Where, Who, and Why? Trends Biochem Sci 43, 211–223. [PubMed: 29398204]

Hingorani SR, Petricoin EF, Maitra A, Rajapakse V, King C, Jacobetz MA, Ross S, Conrads TP, Veenstra TD, Hitt BA, et al. (2003). Preinvasive and invasive ductal pancreatic cancer and its early detection in the mouse. Cancer Cell 4, 437–450. [PubMed: 14706336]

Infante JR, Somer BG, Park JO, Li CP, Scheulen ME, Kasubhai SM, Oh DY, Liu Y, Redhu S, Steplewski K, et al. (2014). A randomised, double-blind, placebo-controlled trial of trametinib, an oral MEK inhibitor, in combination with gemcitabine for patients with untreated metastatic adenocarcinoma of the pancreas. Eur J Cancer 50, 2072–2081. [PubMed: 24915778]

Iwasaki S, and Ingolia NT (2017). The Growing Toolbox for Protein Synthesis Studies. Trends Biochem Sci 42, 612–624. [PubMed: 28566214]

Jackson EL, Willis N, Mercer K, Bronson RT, Crowley D, Montoya R, Jacks T, and Tuveson DA (2001). Analysis of lung tumor initiation and progression using conditional expression of oncogenic K-ras. Genes Dev 15, 3243–3248. [PubMed: 11751630]

Jakobsson ME, Malecki J, and Falnes PO (2018a). Regulation of eukaryotic elongation factor 1 alpha (eEF1A) by dynamic lysine methylation. RNA Biol 15, 314–319. [PubMed: 29447067]

Jakobsson ME, Malecki JM, Halabelian L, Nilges BS, Pinto R, Kudithipudi S, Munk S Davydova E, Zuhairi FR, Arrowsmith CH, et al. (2018b). The dual methyltransferase METTL13 targets N terminus and Lys55 of eEF1A and modulates codon-specific translation rates. Nat Commun 9, 3411. [PubMed: 30143613]

Johnson L, Mercer K, Greenbaum D, Bronson RT, Crowley D, Tuveson DA, and Jacks T (2001). Somatic activation of the K-ras oncogene causes early onset lung cancer in mice. Nature 410, 1111–1116. [PubMed: 11323676]

Kanda M, Matthaei H, Wu J, Hong SM, Yu J, Borges M, Hruban RH, Maitra A, Kinzler K, Vogelstein B, et al. (2012). Presence of somatic mutations in most early-stage pancreatic intraepithelial neoplasia. Gastroenterology 142, 730–733 e739. [PubMed: 22226782]

Kawaguchi Y, Cooper B, Gannon M, Ray M, MacDonald RJ, and Wright CV (2002). The role of the transcriptional regulator Ptf1a in converting intestinal to pancreatic progenitors. Nat Genet 32, 128–134. [PubMed: 12185368]

Lee KE, and Bar-Sagi D (2010). Oncogenic KRas suppresses inflammation-associated senescence of pancreatic ductal cells. Cancer Cell 18, 448–458. [PubMed: 21075310]

Lee MH, and Surh YJ (2009). eEF1A2 as a putative oncogene. Ann N Y Acad Sci 1171, 87–93. [PubMed: 19723040]

Leprivier G, Remke M, Rotblat B, Dubuc A, Mateo AR, Kool M, Agnihotri S, El-Naggar A, Yu B, Somasekharan SP, et al. (2013). The eEF2 kinase confers resistance to nutrient deprivation by blocking translation elongation. Cell 153, 1064–1079. [PubMed: 23706743]

Liu M, Sjogren AK, Karlsson C, Ibrahim MX, Andersson KM, Olofsson FJ, Wahlstrom AM, Dalin M, Yu H, Chen Z, et al. (2010). Targeting the protein prenyltransferases efficiently reduces tumor

development in mice with K-RAS-induced lung cancer. Proceedings of the National Academy of Sciences of the United States of America 107, 6471–6476. [PubMed: 20308544]

Martineau Y, Azar R, Muller D, Lasfargues C, El Khawand S, Anesia R, Pelletier J, Bousquet C, and Pyronnet S (2014). Pancreatic tumours escape from translational control through 4E-BP1 loss. Oncogene 33, 1367–1374. [PubMed: 23563181]

Mazur PK, Herner A, Mello SS, Wirth M, Hausmann S, Sanchez-Rivera FJ, Lofgren SM, Kuschma T, Hahn SA, Vangala D, et al. (2015). Combined inhibition of BET family proteins and histone deacetylases as a potential epigenetics-based therapy for pancreatic ductal adenocarcinoma. Nat Med 21, 1163–1171. [PubMed: 26390243]

Mazur PK, Reynoird N, Khatri P, Jansen PW, Wilkinson AW, Liu S, Barbash O, Van Aller GS, Huddleston M, Dhanak D, et al. (2014). SMYD3 links lysine methylation of MAP3K2 to Ras-driven cancer. Nature 510, 283–287. [PubMed: 24847881]

Morgens DW, Wainberg M, Boyle EA, Ursu O, Araya CL, Tsui CK, Haney MS, Hess GT, Han K, Jeng EE, et al. (2017). Genome-scale measurement of off-target activity using Cas9 toxicity in high-throughput screens. Nat Commun 8, 15178. [PubMed: 28474669]

Morgenstern JP, and Land H (1990). Advanced mammalian gene transfer: high titre retroviral vectors with multiple drug selection markers and a complementary helper-free packaging cell line. Nucleic Acids Res 18, 3587–3596. [PubMed: 2194165]

Morris J.P.t., Cano DA, Sekine S, Wang SC, and Hebrok M (2010). Beta-catenin blocks Kras-dependent reprogramming of acini into pancreatic cancer precursor lesions in mice. J Clin Invest 120, 508–520. [PubMed: 20071774]

Murn J, and Shi Y (2017). The winding path of protein methylation research: milestones and new frontiers. Nat Rev Mol Cell Biol 18, 517–527. [PubMed: 28512349]

Orimo A, Gupta PB, Sgroi DC, Arenzana-Seisdedos F, Delaunay T, Naeem R, Carey VJ, Richardson AL, and Weinberg RA (2005). Stromal fibroblasts present in invasive human breast carcinomas promote tumor growth and angiogenesis through elevated SDF-1/CXCL12 secretion. Cell 121, 335–348. [PubMed: 15882617]

Robichaud N, Sonenberg N, Ruggero D, and Schneider RJ (2018). Translational Control in Cancer. Cold Spring Harb Perspect Biol.

Ruggero D, Montanaro L, Ma L, Xu W, Londei P, Cordon-Cardo C, and Pandolfi PP (2004). The translation factor eIF-4E promotes tumor formation and cooperates with c-Myc in lymphomagenesis. Nat Med 10, 484–486. [PubMed: 15098029]

Sanjana NE, Shalem O, and Zhang F (2014). Improved vectors and genome-wide libraries for CRISPR screening. Nat Methods 11, 783–784. [PubMed: 25075903]

Schmidt EK, Clavarino G, Ceppi M, and Pierre P (2009). SUnSET, a nonradioactive method to monitor protein synthesis. Nat Methods 6, 275–277. [PubMed: 19305406]

Schuller AP, and Green R (2018). Roadblocks and resolutions in eukaryotic translation. Nat Rev Mol Cell Biol 19, 526–541. [PubMed: 29760421]

Stewart SA, Dykxhoorn DM, Palliser D, Mizuno H, Yu EY, An DS, Sabatini DM, Chen IS, Hahn WC, Sharp PA, et al. (2003). Lentivirus-delivered stable gene silencing by RNAi in primary cells. RNA 9, 493–501. [PubMed: 12649500]

Truitt ML, Conn CS, Shi Z, Pang X, Tokuyasu T, Coady AM, Seo Y, Barna M, and Ruggero D (2015). Differential Requirements for eIF4E Dose in Normal Development and Cancer. Cell 162, 59–71. [PubMed: 26095252]

Truitt ML, and Ruggero D (2016). New frontiers in translational control of the cancer genome. Nat Rev Cancer 16, 288–304. [PubMed: 27112207]

Van Noort JM, Kraal B, Sinjorgo KM, Persoon NL, Johanns ES, and Bosch L (1986). Methylation in vivo of elongation factor EF-Tu at lysine-56 decreases the rate of tRNA-dependent GTP hydrolysis. Eur J Biochem 160, 557–561. [PubMed: 3096728]

Zhu L, Shi G, Schmidt CM, Hruban RH, and Konieczny SF (2007). Acinar cells contribute to the molecular heterogeneity of pancreatic intraepithelial neoplasia. Am J Pathol 171, 263–273. [PubMed: 17591971]
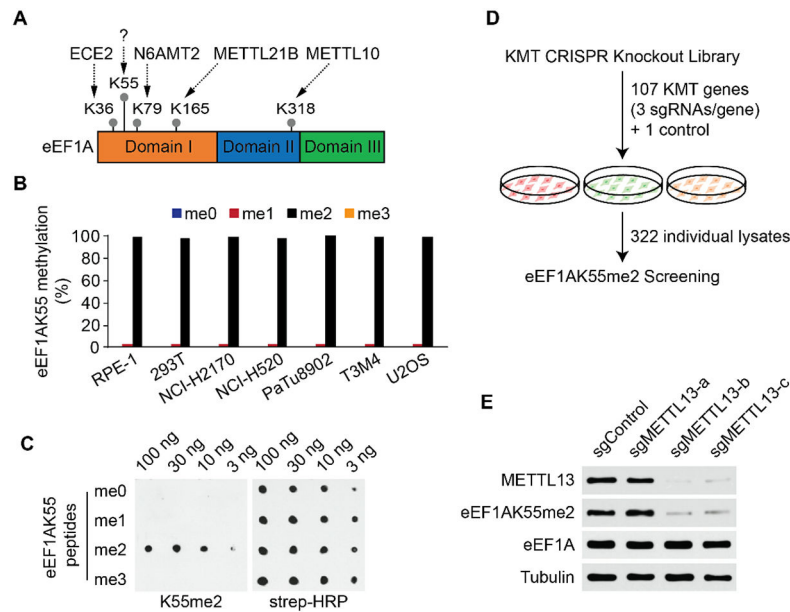
Figure 1. Identification of METTL13 as a Candidate eEF1A Lysine 55 Methyltransferase.
(**A**) Schematic of human eEF1A with the indicated major lysine methylation sites and protein domains. Methylated lysine residues are indicated by grey dots. Arrows connect the enzyme responsible for methylation with the indicated lysine residue. The "?" indicates that the enzyme for generating K55 methylation is unknown.

(**B**) eEF1AK55 is primarily di-methylated in human cell lines. Quantitative analysis of endogenous eEF1AK55 methylation levels in the indicated cell lines by mass spectrometry.

(**C**) Specific recognition of eEF1AK55me2 peptides by the anti-eEF1AK55me2 antibody. Dot blot analysis with αeEF1AK55me2 antibody (K55me2) using the indicated biotinylated peptides. Blots probed with HRP-conjugated streptavidin (strep-HRP) shown as loading controls.

(**D**) Schematic of gene editing-coupled biochemical screening strategy to discover candidate KMT/s responsible for eEF1AK55 methylation. See Table S1 for list of the 322 sgRNAs.

(**E**) Identification of METTL13 as a putative eEF1AK55 methyltransferase. Western analysis with the indicated antibodies of U2OS whole cell lysates expressing CRISPR/Cas9 and three independent sgRNAs targeting METTL13 (as in Figure S1F) and the control sgRNA (as in Figure S1E). Total eEF1A levels do no change and tubulin is shown as a loading control.

See also Figure S1, Table S1
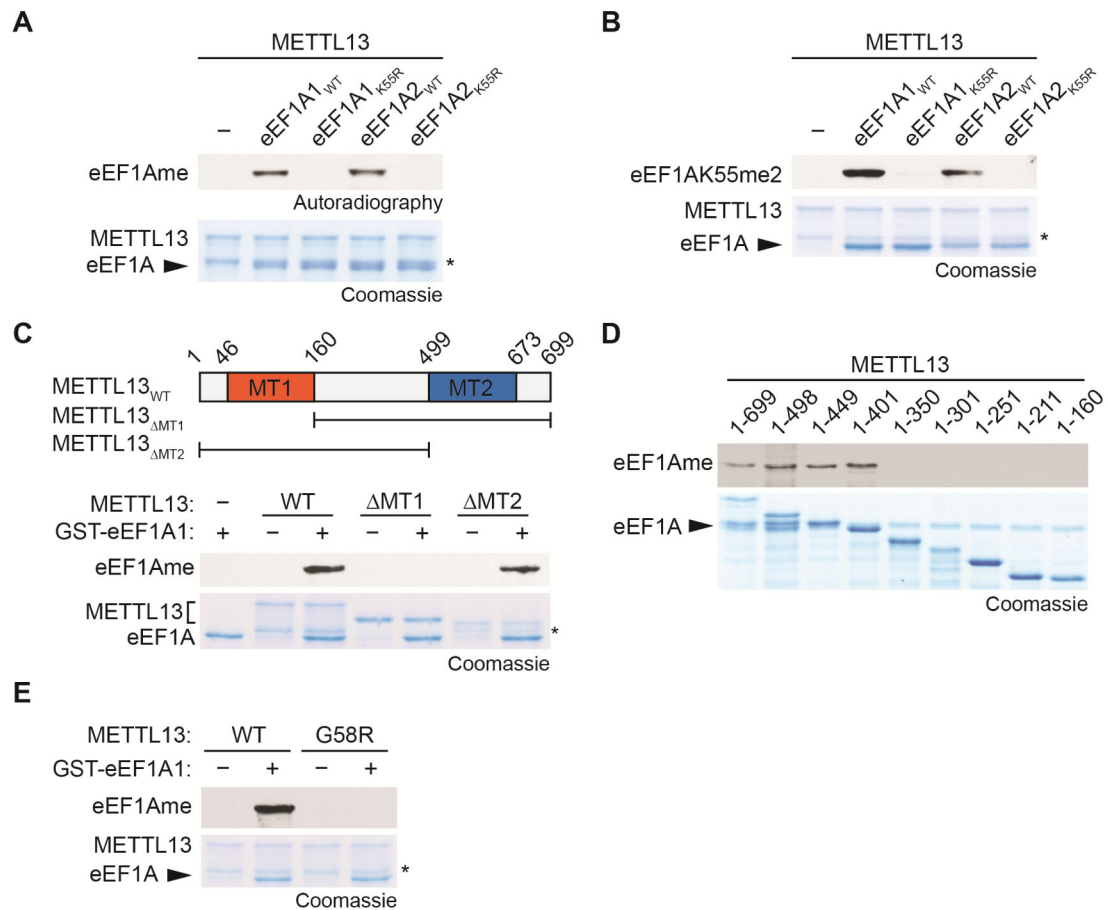
Figure 2. *In vitro* Methylation of eEF1A at Lysine 55 by METTL13.

(**A**) *In vitro* methylation assay with recombinant METT13 and recombinant wild-type GST-eEF1A1/2 or K55R mutants as indicated. Top panel, ^{3}H-SAM is the methyl donor and methylation visualized by autoradiography. Bottom panel, Coomassie stain of proteins in the reaction. Asterisk in (A-C, E) indicates METTL13 breakdown product.

(**B**) *In vitro* methylation assay as in (A) with non-radiolabeled SAM. Top panel, Western analysis with anti-eEF1AK55me2. Bottom panel, Coomassie stain of proteins in the reaction.

(**C**) The N-terminal MT1 domain of METTL13 is necessary for eEF1AK55 methylation. *In vitro* methylation assay on GST-eEF1A1 with recombinant wild-type METTL13 or the indicated domain deletion fragments. Top panel, schematic diagram of putative methyltransferase (MT) domains of METTL13 and the truncated fragments used in methylation assays. Middle panel, autoradiogram of methylation assay. Bottom panel, Coomassie stain of proteins in the reaction.

(**D**) Amino acids 1-401 of METTL13 are sufficient for eEF1AK55 methylation. *In vitro* methylation assay on GST-eEF1A1 with wild-type METTL13 or the indicated METTL13 truncated proteins. Top panel, autoradiogram of methylation assay. Bottom panel, Coomassie stain of proteins in the reaction.
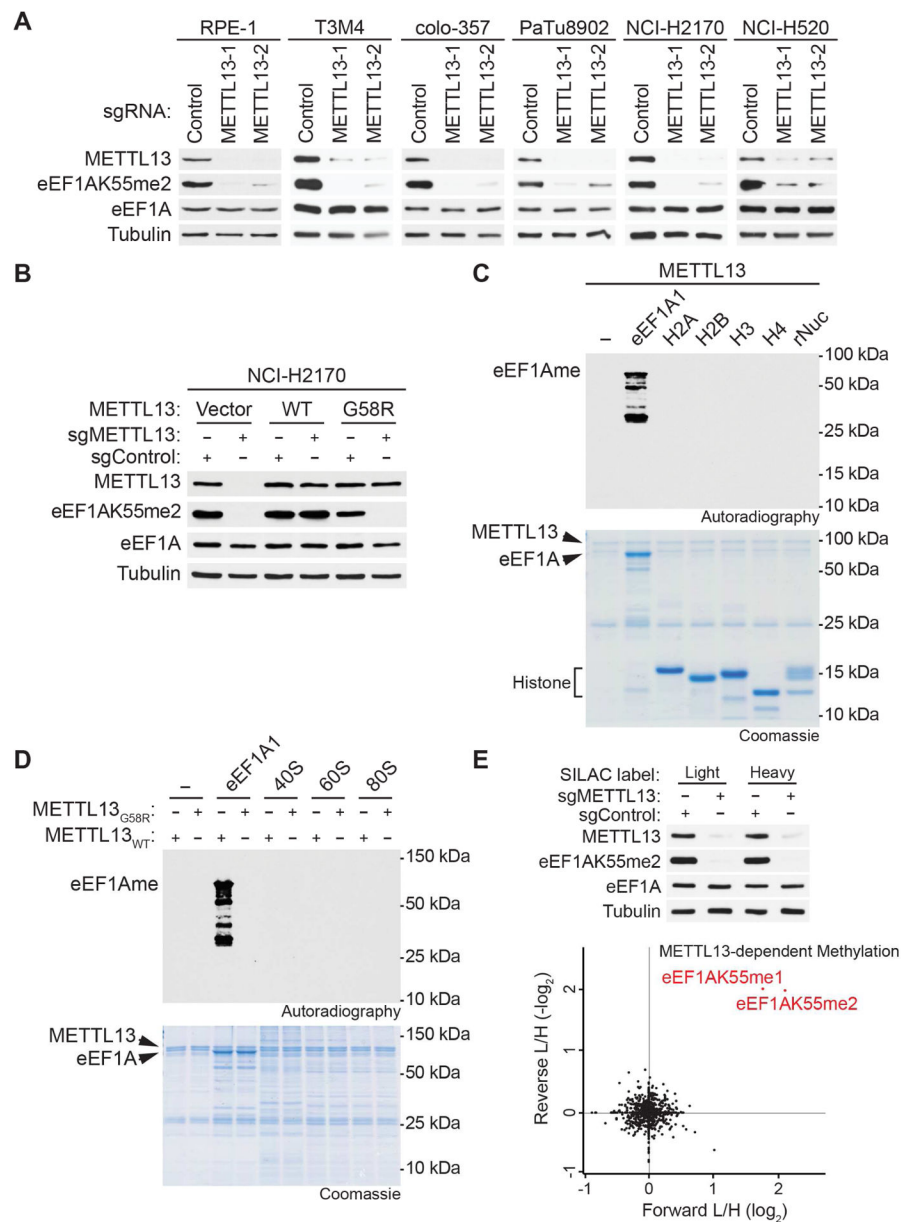
(**E**) Identification of METTL13 catalytic mutant. *In vitro* methylation assay on GST-eEF1A1 with wild-type METTL13 or METTL13 G58R mutant. Top panel, autoradiogram of methylation assay. Bottom panel, Coomassie stain of proteins in the reaction.

See also Figure S2

A

B

C

D

E

Figure 3. The Principal Physiologic Activity of METTL13 is eEF1AK55 Methylation.

(**A**) METTL13 is required for eEF1AK55 methylation in multiple human cell lines. Western analysis with the indicated antibodies of whole cell extracts (WCEs) from the indicated cell lines (see methods) expressing two independent sgRNAs targeting METTL13 or a control sgRNA.

(**B**) Reconstitution with wild-type METTL13 but not the inactive mutant restores EF1AK55me2 in cells. Western analysis with the indicated antibodies of WCEs from wild-type or METTL13-deficient NCI-H2170 cells complemented with CRISPR-resistant METTL13 (WT or G58R), or control as indicated.

(**C**) Histones and nucleosomes are not methylated by METTL13. *In vitro* methylation assay as in Figure 2 on recombinant GST-eEF1A1, core histones (H2A, H2B, H3, and H4) or recombinant nucleosome (rNuc) with METTL13. eEF1A breakdown products containing

K55 are seen below full-length with long exposure. Top panel, autoradiogram of methylation assay. Bottom panel, Coomassie stain of proteins in the reaction.

(**D**) Purified ribosomes are not methylated by METTL13. *In vitro* methylation assay as in (C) on recombinant GST-eEF1A1, 40S and 60S ribosomal subunits, and 80S ribosomes isolated from cytoplasmic extracts of T3M4 cells with indicated METTL13 protein.

(**E**) Methylation of eEF1AK55 is the only change out of >1000 methylated events detected upon METTL13 depletion in cells. Top panel, Western analysis with the indicated antibodies of WCEs from control or METTL13-depleted T3M4 cells maintained in SILAC media. Bottom panel, SILAC-based quantitative proteomic analysis of methylated peptides in cells ±METTL13. Methylated peptides are plotted by their SILAC ratios in two independent experiments in the forward (x axis) and reverse (y axis) experiments. Any methylated peptide that is dependent upon METTL13 will reside in the top right quadrant. Of the >1000 methylated peptides detected in the analysis (see Table S2), only the two eEF1A peptides harboring K55me1 and K55me2 are present in the top right quadrant as indicated in red. L/H, light over heavy fraction ratio.

See also Figure S3, Table S2
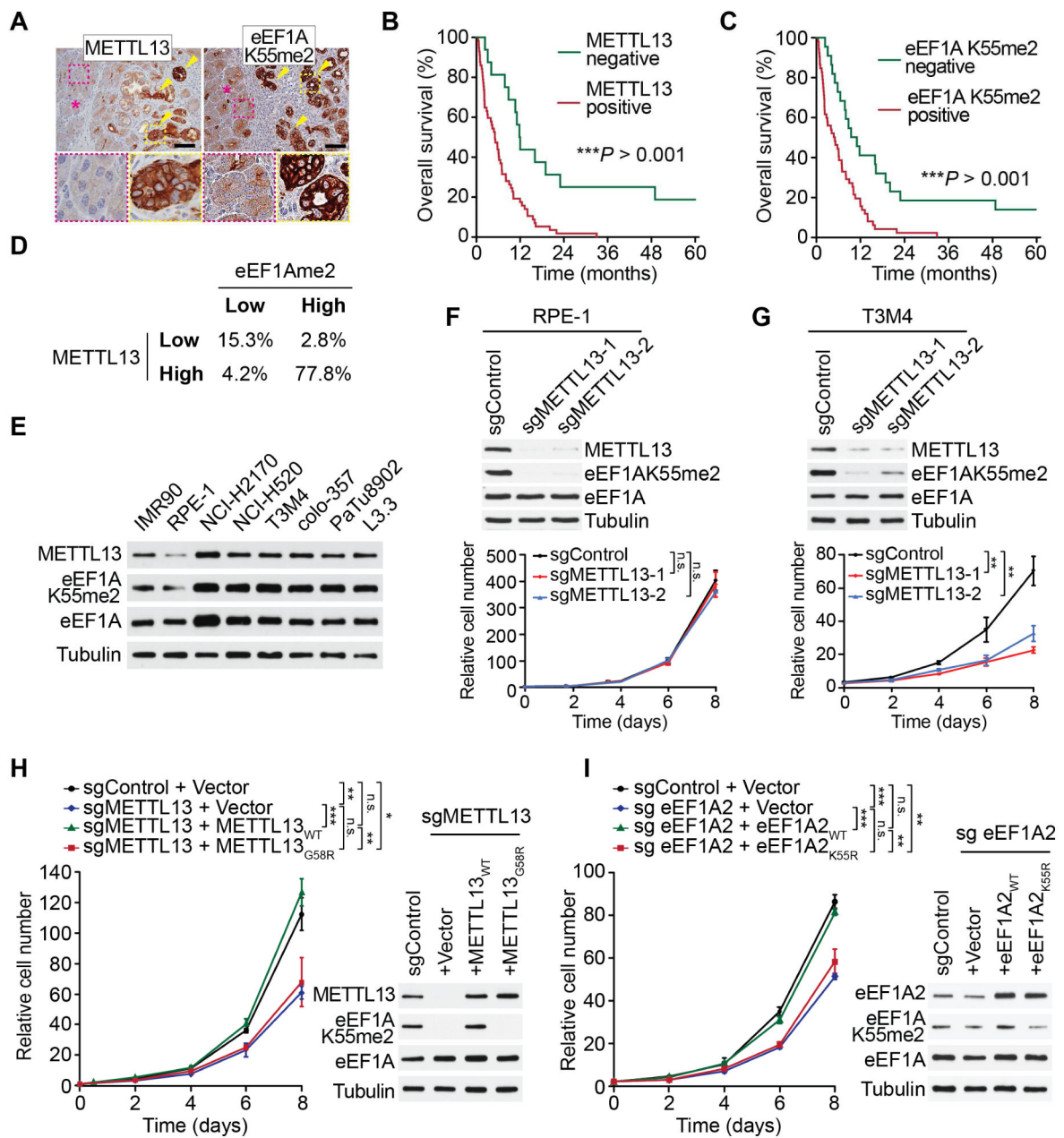
Figure 4. METTL13 and eEF1AK55me2 Promote Cancer Cell Proliferation.

(**A**) Representative IHC images showing METTL13 and eEF1AK55me2 expression in pancreatic cancer lesions (arrowheads) but not in adjacent normal acini (asterisk) in human tissue samples (representative of 12 independent samples). Scale bars, 100 μm. The area marked with dotted lines is presented at higher magnification in the insets.

(**B** and **C**) Analysis of correlation of METTL13 (B) and eEF1AK55me2 (C) staining and PDAC patient survival assessed by IHC. $***P < 0.001$, log-rank test, 72 different samples were stained in total for each antibody, a representative staining presented on the right. Scale bars: 100 μm.

(**D**) Correlation analysis of METTL13 and eEF1AK55me2 IHC signal (from **B-C** and S4E-F). Spearman correction r = 0.715, *P*-value < 0.0001, data presented as percent of samples in each category (see Methods).

(**E**) Upregulation of METTL13 expression and eEF1AK55me2 levels in pancreatic and lung cancer cells compared to non-transformed cell lines. Western analysis with the indicated antibodies of WCEs from the indicated cell lines. IMR90 are normal human fibroblasts, RPE-1 are immortalized non-transformed human epithelial cells. Tubulin is shown as a loading control.

(**F** and **G**) METTL13 depletion inhibits cell proliferation in a PDAC cell line but not in non-transformed cells. Western analysis (top pane) of WCEs and cell proliferation rates (bottom panel) of the non-transformed cell line RPE-1 (**F**) and human PDAC cell line T3M4 (**G**) expressing two independent METTL13 sgRNAs or a control sgRNA. Error bars represent S.D. from three independent experiments. **P < 0.01, n.s., not significant, two-tailed unpaired Student's t-test.

(**H**) METTL13 catalytic activity is required for METTL13-dependent proliferation of T3M4 cells. Western analysis and cell proliferation rates as in (**G**) of control or METTL13-depleted T3M4 cells complemented with CRISPR-resistant METTL13$_{WT}$, METTL13$_{G58R}$ or control. Error bars represent S.D. from three independent experiments. *P < 0.05, **P < 0.01, ***P < 0.001, n.s., not significant, two-tailed unpaired Student's t-test.

(**I**) Role for intact K55 on eEF1A2 in promoting T3M4 proliferation. Western analysis and cell proliferation rates as in (**G**) of eEF1A2-depleted T3M4 cells complemented with CRISPR-resistant eEF1A2$_{WT}$, eEF1A2$_{K55R}$ or control. Error bars represent S.D. from three independent experiments. **P < 0.01, ***P < 0.001, n.s., not significant, two-tailed unpaired Student's t-test.

See also Figure S4
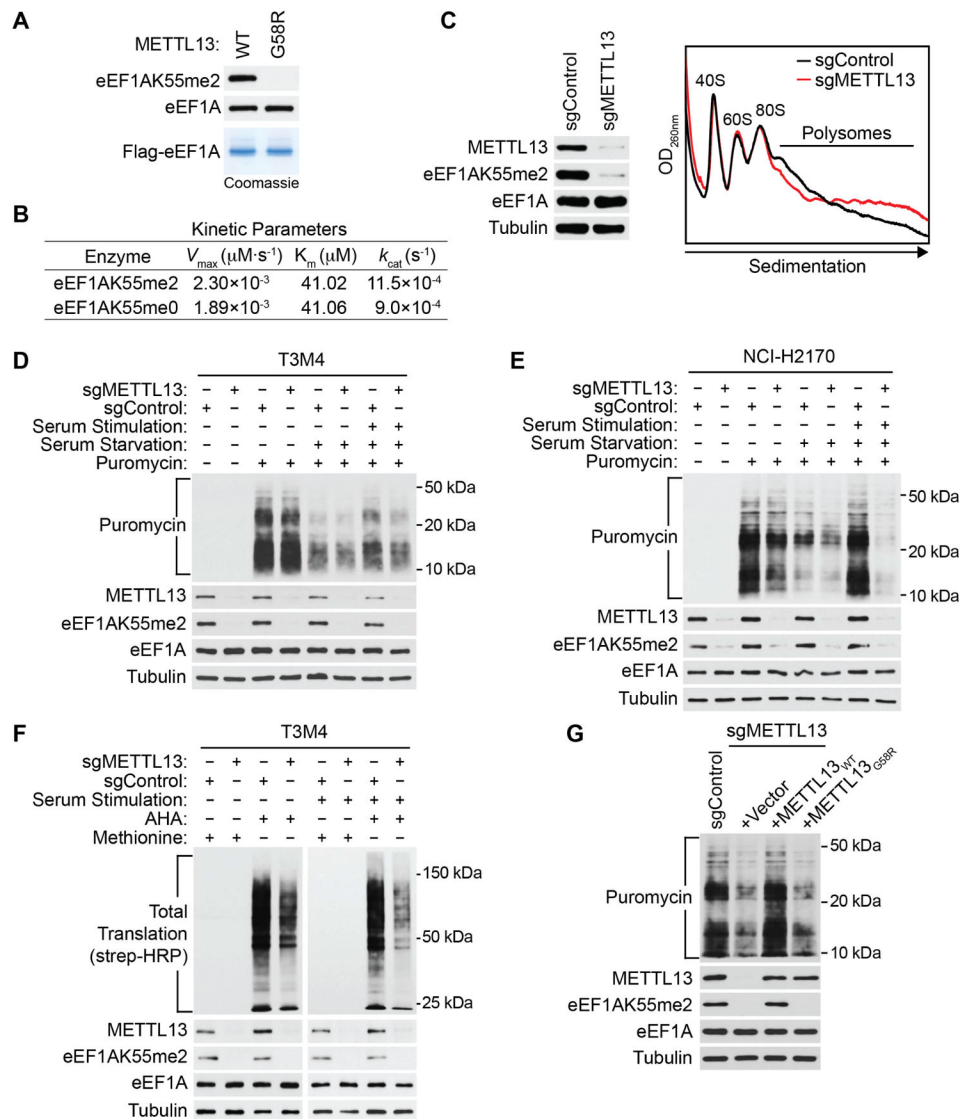
Figure 5. METTL13-mediated eEF1AK55 Dimethylation Enhances Protein Synthesis in Cells.
(**A**) Purification of recombinant eEF1A1 ±K55me2. Top and middle panels, Western analysis with the indicated antibodies of eEF1A purified from 293T cells ±catalytically active METTL13 as indicated. Bottom panel, Coomassie stain of purified eEF1A1.
(**B**) K55me2 increases the catalytic efficiency of GTP hydrolysis by eEF1A. The Michaelis-Menten kinetic parameters of Flag-eEF1A1 ±K55me2 purified from (A) are shown.
(**C**) Cytosolic extracts were isolated from control or METTL13-depleted T3M4 cells and fractionated on 5-50% sucrose gradients. Absorbance profiles show distribution of 40 and 60S ribosomal subunits, 80S monosome and polysomes. OD_{260nm}, optical density at 260 nm. Left panel, Western analysis represents WCEs from the indicated cell lines used for the polysome profiling.
(**D** and **E**) SUnSET assays under the indicated conditions reveal reduced protein production in METTL13-depleted T3M4 (D) and NCI-H2170 (E) cells. WCEs were isolated and probed the indicated antibodies.

(**F**) AHA labeling under the indicated conditions shows decrease in protein synthesis upon depletion of METTL13 in T3M4 cells. WCE of T3M4 probed with the indicated antibodies.

(**G**) METTL13's catalytic activity is required for enhanced protein synthesis in cells. SUnSET assays as in (D) of control (sgControl plus vector control) or METTL13-depleted T3M4 cells complemented with CRISPR-resistant METTL13$_{WT}$, METTL13$_{G58R}$ or control as indicated and after recovery from serum starvation. WCEs were isolated and probed the indicated antibodies.

See also Figure S5
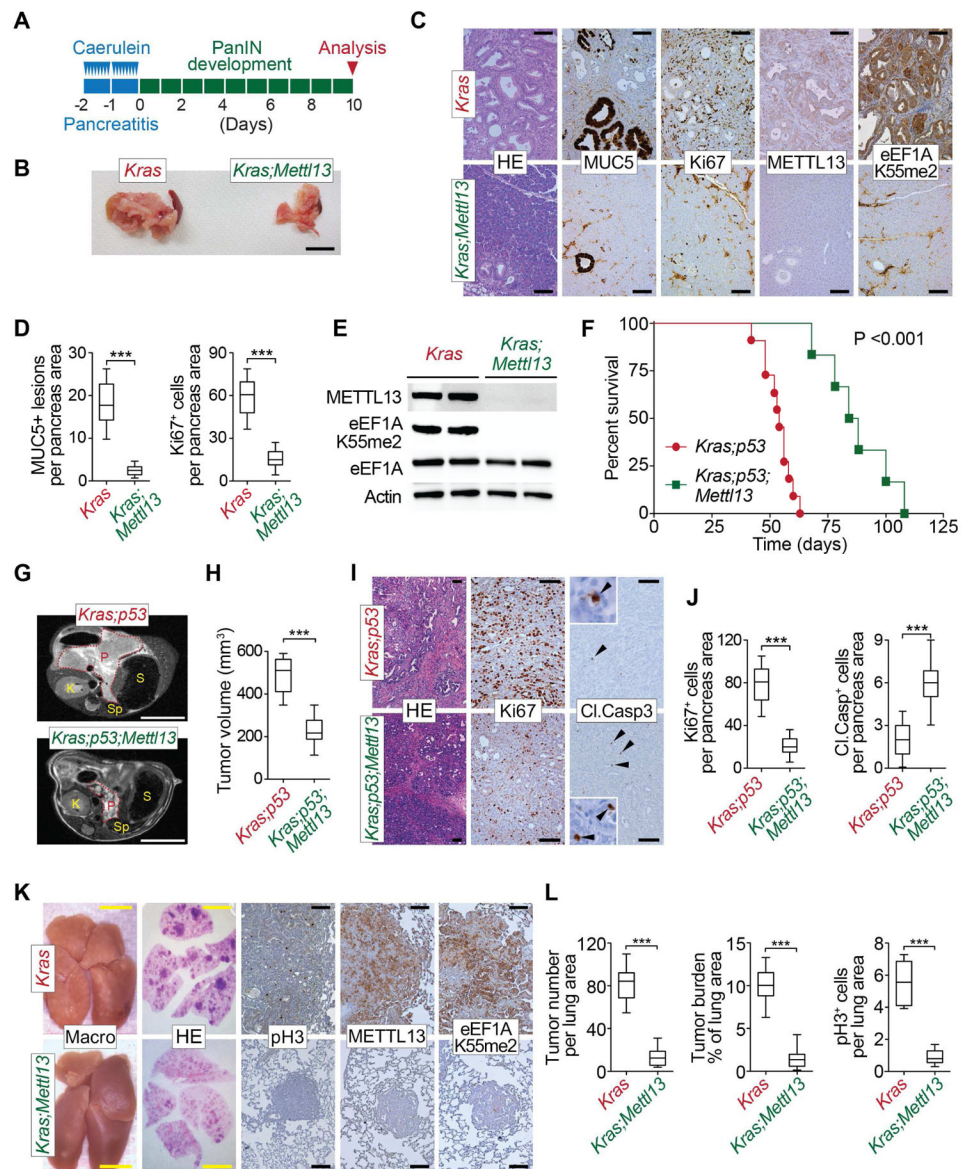
Figure 6. METTL13 Deletion Represses KRAS-driven Pancreatic and Lung Tumorigenesis In Vivo.

(**A**) Schematic of the caerulein pancreatitis-induced precancerous (PanINs) lesion formation protocol used in *Kras;Mettl13* and *Kras* (control) mice.

(**B**) Representative examples of pancreata gross images (representative of 12 independent samples). Scale bar, 1 cm.

(**C**) Representative haematoxylin and eosin (HE) staining and IHC for MUC5, a marker of PanIN lesions, Ki67, a marker of cell proliferation, METTL13 and eEF1AK55me2 (representative of 12 independent samples). Scale bars, 100 μm.

(**D**) Quantification of Ki67-positive proliferating cell and MUC5-positive lesions in caerulein-treated pancreata from *Kras* control (n = 12) and *Kras;Mettl13* (n = 12). ***P < 0.001, two-tailed unpaired Student's t-test. Data are represented as mean ± s.e.m.

(**E**) Westerns with the indicated antibodies of pancreatic tissue lysates from *Kras;Mettl13* and *Kras* (control) mutant mice (two independent and representative samples are shown for each genotype).

(**F**) Kaplan-Meier survival curves of *Kras;p53* control mice (n = 10, median survival = 54 d) and *Kras;p53;Mettl13* mutant mice (n = 6, median survival = 86 d). ***$P < 0.001$, log-rank test for significance.

(**G**) Representative MRI scan in 7th week to analyze tumor volume in *Kras;p53;Mettl13* and *Kras;p53* mutant mice. Red dotted lines indicate pancreas area; abbreviations used: P=pancreas, S=stomach, K=kidney, Sp=spleen. Scale bars, 1cm.
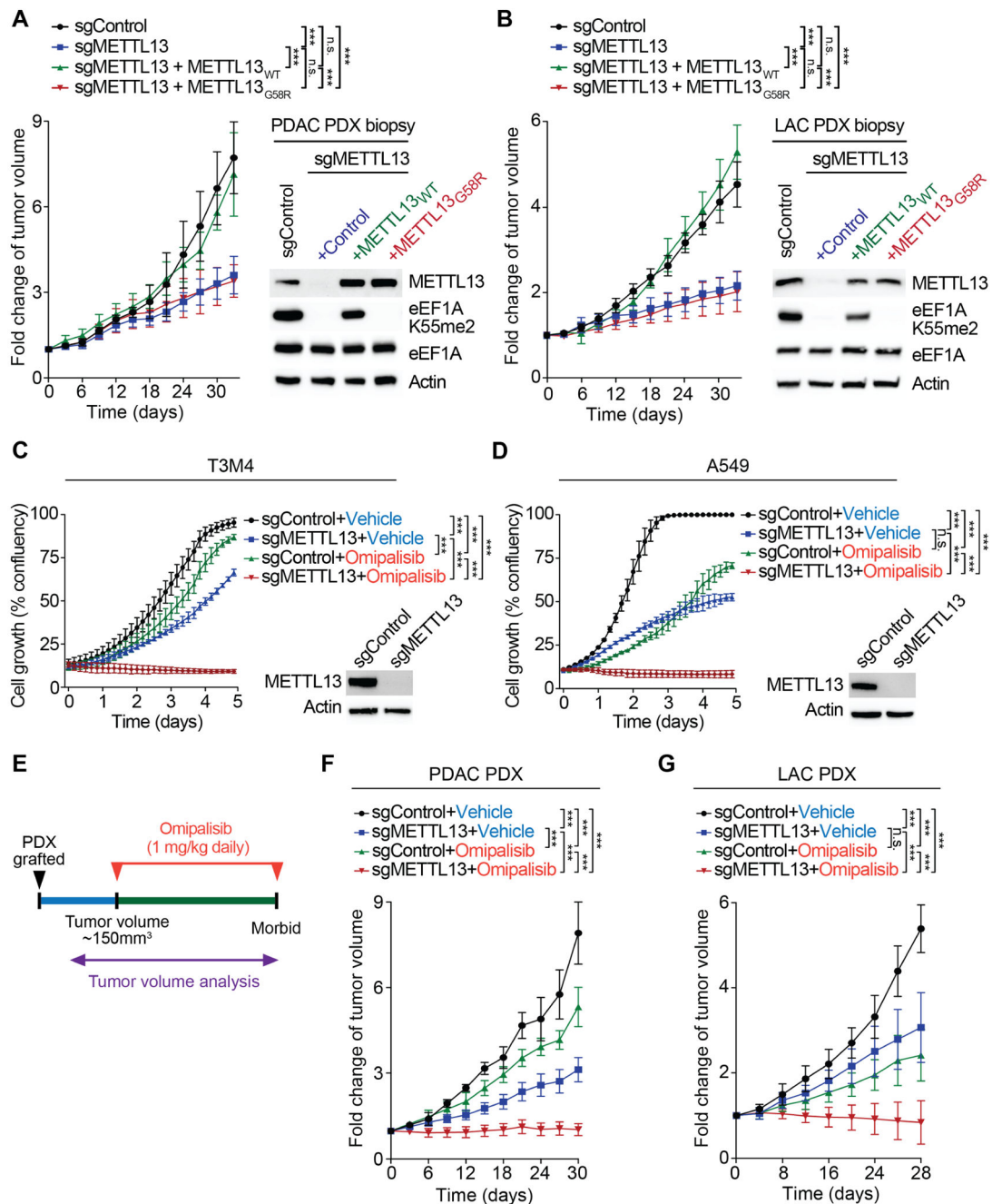
(**H**) Tumor/pancreas volume quantification in 7th week of age based on MRI scan (detailed procedure in Methods) of *Kras;p53;Mettl13* and *Kras;p53* mice (n = 4, each genotype) ***$P < 0.001$, two-tailed unpaired Student's t-test. Data are represented as mean ± s.e.m.

(**I**) Representative HE and IHC for Ki67 (a maker of proliferation) and Cleaved Caspase 3 (Cl.Casp 3, a marker of apoptosis) in pancreas tumors at autopsy in *Kras;p53;Mettl13* and *Kras;p53* mutant mice. Scale bars, 100 μm, insets magnification x10.

(**J**) Quantification of Ki67-positive proliferating cell and Cleaved Caspase 3 apoptotic cells in pancreata at autopsy from *Kras;p53* control (n = 6) and *Kras;p53;Mettl13* (n = 6) mutant mice. ***$P < 0.001$, two-tailed unpaired Student's t-test. Data are represented as mean ± s.e.m.

(**K**) Representative macroscopic picture of lungs, HE staining and IHC for phospho-Histone H3 (pH3, a marker of proliferation), METTL13 and eEF1AK55me2 (representative of 8 independent samples). Scale bars: yellow 1 cm; black 100 μm.

(**L**) Quantification of tumor number, tumor area (burden) and phospho Histone H3-positive (pH3+) proliferating cells per lung area in *Kras* control (n = 8) and *Kras;Mettl13* (n = 8). ***$P < 0.001$, two-tailed unpaired Student's t-test. Data are represented as mean ± s.e.m. See also Figure S6

Figure 7. Depletion of METTL13's Catalytic Activity Inhibits Growth of Pancreatic and Lung Cancer PDX Tumors *in vivo* and Regression of PDX Tumors by METTL13 Depletion and PI3K/mTOR Inhibitors.

(**A**) Tumor volume quantification for patient derived PDAC xenografts modified to express sgRNA METTL13 or sgRNA control and overexpressing METTL13$_{WT}$ or catalytically deficient METTL13$_{G58R}$ in mice (n = 8 mice for each treatment group). ***$P < 0.001$, two-tailed unpaired Student's t-test. Data are represented as mean ± s.e.m. Westerns with the indicated antibodies of PDX biopsies (one representative sample for each condition is shown).

(**B**) Tumor volume quantification for patient derived LAC xenografts modified to express sgRNA METTL13 or sgRNA control and overexpressing METTL13$_{WT}$ or METTL13$_{G58R}$ in mice (n = 8 mice for each treatment group). ***P < 0.001, two-tailed unpaired Student's t-test. Data are represented as mean ± s.e.m. Westerns with the indicated antibodies of PDX biopsies (one representative sample for each condition is shown).

(**C**) Population growth of T3M4 pancreatic cancer cell line depleted for METTL13 by CRISPR/Cas9 sgRNA (sgMETTL13) or control (sgControl). Confluency of cells over 96h treated with Omipalisib (1μM) or placebo (vehicle). ***P < 0.001, two-tailed unpaired Student's t-test. Data are represented as mean ± s.e.m (three independent experiments). Westerns of WCE with the indicated antibodies are shown.

(**D**) Population growth of A549 lung cancer cell line depleted for METTL13 by CRISPR/Cas9 sgRNA (sgMETTL13) or control (sgControl) as in (C). ***P < 0.001, two-tailed unpaired Student's t-test. Data are represented as mean ± s.e.m (three independent experiments). Westerns of WCE with the indicated antibodies are shown.

(**E**) Treatment schedule for administration of Omipalisib (GSK2126458, 1 mg kg–1, intraperitoneal injection once daily) to immunocompromised mice grafted with PDX pancreatic (see F) or lung cancer (see G). Control mice received placebo (vehicle). Treatment started when tumors were around 150 mm^3.

(**F** and **G**) Tumor volume quantification for patient derived (C) PDAC and (D) LAC xenografts modified to express sgRNA METTL13 or sgRNA Control treated with placebo (vehicle) or Omipalisib. Plots showing fold change in tumor volume compared to initial tumor volume. ***P < 0.001, n.s., not significant, two-tailed unpaired Student's t-test. Data are represented as mean ± s.e.m.

See also Figure S7, Table S3

KEY RESOURCES TABLE

REAGENT OR RESOURCE	SOURCE	IDENTIFIER
Antibodies		
β-actin	Sigma-Aldrich	Cat# A4700
MUC5AC	Thermo Fisher Scientific	Cat# 145P1
Ki67	BD Bioscience	Cat# 550609
Phospho-Histone H 3	Millipore	Cat# 06-570
Cleaved Caspase 3	Cell Signaling Technologies	Cat# 9664
CK19	Developmental Studies Hybridoma Bank	Cat# TromaIII
anti-Mouse HRP	Cell Signaling Technologies	Cat# 7076
anti-Rabbit HRP	Cell Signaling Technologies	Cat# 7074
eEF1AK55me1	ABclonal Biotechnology	N/A
eEF1AK55me2	ABclonal Biotechnology	N/A
eEF1AK55me3	ABclonal Biotechnology	N/A
eEF1A	Millipore	Cat# 05-235
β-tubulin	Millipore	Cat# 05-661
puromycin	Millipore	Cat# MABE343
METTL13	Bethyl Laboratories	Cat# A304-194A
peroxidase-conjugated streptavidin	Jackson ImmunoResearch	Cat# 016-030-084
eEF1A2	Abnova	Cat# H00001917-A01
eIF3A	Abcam	Cat# ab86146
RPS6	Abcam	Cat# ab70227
RPL6	Abcam	Cat# ab126100
CD45-Biotin	eBiosciences	Cat# 13-0451-81
CD31-Biotin	eBiosciences	Cat# 13-0319-80
Ter119-Biotin	eBiosciences	Cat# 13-5921-81
Biotin Micro Beads	Miltenyi Biotec	Cat# 130-042-401
Bacterial and Virus Strains		
One Shot TOP10	Invitrogen	Cat# C404003
Adenovirus-Cre	Baylor College of Medicine, Viral Vector Production Core	Cat# Ad5-CMV-Cre
DH5α	Thermo Fisher Scientific	Cat# K4520-1
BL21	Thermo Fisher Scientific	Cat# C6070-03
Biological Samples		
Human PDAC and LAC Tissue Array	MD Anderson Pathology	N/A
Chemicals, Peptides, and Recombinant Proteins		
Geneticin	Thermo Fisher Scientific	Cat# 10131027
Blasticidin S	Thermo Fisher Scientific	Cat# R21001
Puromycin	Thermo Fisher Scientific	Cat# A1113802
Hygromycin B	Corning	Cat# 30240CR
G418 Sulfate	Corning	Cat# MT30234CI
MACS separation columns	Miltenyi Biotech	Cat# 130-042-401

REAGENT OR RESOURCE	SOURCE	IDENTIFIER
Complete Protease Inhibitor Cocktail	Sigma-Aldrich	Cat# 4693159001
Phosphatase Inhibitor Cocktail	Thermo Fisher Scientific	Cat# 78420
Hydrogen Peroxide	Thermo Fisher Scientific	Cat# H325-500
Sequencing Grade Modified Trypsin	Promega	Cat# V5113
Glu-C	Promega	Cat# V1651
Collagenase-VIII	Sigma-Aldrich	Cat# C2139
TRIzol Reagent	Invitrogen	Cat# 15596018
Forane (Isoflurane)	AbbVie	Cat#B506
Caerulein	Sigma-Aldrich	Cat# C9026
Soybean trypsin inhibitor	Sigma-Aldrich	Cat# T6522
Rat Tail Collagen	Corning	Cat# 354236
Recombinant mouse EGF	Thermo Fisher Scientific	Cat# PMG8044
Bovine Serum Albumin (BSA)	Thermo Fisher Scientific	Cat# BP9703100
TransIT-293	Mirus Bio	Cat# MIR-2706
SUPERase In RNase Inhibitor	Thermo Fisher Scientific	Cat# AM2694
RNasin Ribonuclease Inhibitors	Promega	Cat# N2511
GTP solution	Thermo Fisher Scientific	Cat# R1461
L-lysine-2HCl	Thermo Fisher Scientific	Cat# 88429
L-arginine-HCl	Thermo Fisher Scientific	Cat# 88427
L-proline	Thermo Fisher Scientific	Cat# 88430
$^{13}C_6$, $^{15}N_2$-L-lysine HCl	Silantes GmbH	Cat# 211604102
$^{13}C_6$, $^{15}N_4$-L-arginine HCl	Silantes GmbH	Cat# 201604102
l-azidohomoalanine (AHA)	Click Chemistry Tools	Cat# 1066-100
Biotin-PEG4-Alkyne	Click Chemistry Tools	Cat# TA105-25
Peptides: AEMGKGSFXYAWVLDKLKGGK-biotin (X=Kme0, Kme1, Kme2, Kme3)	Chinapeptides	N/A
Critical Commercial Assays		
RNeasy Mini Kit	Qiagen	Cat#74106
ZymoPURE Plasmid Miniprep Kit	Zymo	Cat# D4211
ZymoPURE II Plasmid Maxiprep Kit	Zymo	Cat# D4203
DAB Substrate Kit	Abcam	Cat# ab64238
Vectastain ABC kit	Vector Laboratories	Cat# PK-6100
BCA Protein Assay Kit	Pierce	Cat# 23227
ECL Substrate	Amersham	Cat# RPN2106
PCR Mycoplasma Test Kit I/C	PromoKine	Cat# PK-CA91-1096
ATPase/GTPase Activity Assay Kit	Sigma	Cat# MAK113-1KT
Cell Proliferation ELISA BrdU (colorimetric)	Roche	Cat# 11647229001
Coomassie Plus assay	Thermo Fisher Scientific	Cat# 23236
InstantBlue Protein Stain	Expedeon	Cat# ISB1L
SilverQuest Silver Staining Kit	Thermo Fisher Scientific	Cat# LC6070
Click Chemistry Reaction Buffer Kit	Click Chemistry Tools	Cat# 1001
Site-directed mutagenesis kit	Agilent	Cat# 200523

REAGENT OR RESOURCE	SOURCE	IDENTIFIER
MACS LS column	Miltenyi Biotec	Cat# 130-042-401
Experimental Models: Cell Lines		
Human: 293T/17 cells	ATCC	Cat# CRL-11268
U2OS	ATCC	Cat# HTB-96
hTERT RPE-1	ATCC	Cat# CRL-4000
A549	ATCC	Cat# CCL-185
T3M4	Riken	Cat# RCB1021
PaTu8902	DSMZ	Cat# ACC 179
Colo-357	ECACC	Cat# 94072245
L3.3	RRID	Cat# CVCL_8147
NCI-H520	ATCC	Cat# HTB-182
NCI-H2170	ATCC	Cat# CRL-5928
HT1080	ATCC	Cat# CCL-121
IMR90	ATCC	Cat# CCL-186
Experimental Models: Organisms/Strains		
Mouse: $Kras^{LSL-G12D}$	The Jackson Laboratories	Strain# 008179
Mouse: $p53^{lox/lox}$	The Jackson Laboratories	Strain# 008462
Mouse: $Ptf1a^{Cre}$	(Kawaguchi et al., 2002)	MGI# 2387812
Mouse: $Mettl13^{lox/lox}$	In this study	N/A
Mouse: $NOD.SCID-IL2Rg^{-/-}$ (NSG)	The Jackson Laboratories	Strain# 005557
Oligonucleotides		
sgRNA: Control: 5'-CTTCGAAATGTCCGTTCGGT-3'	This paper	N/A
sgRNA: METTL13-1: 5'-GGATGTGTCTCACAAAGGTG-3'	This paper	N/A
sgRNA: METTL13-2: 5'-CTGAAGGATGTGTCTCACAA-3'	This paper	N/A
sgRNA: eEF1A2: 5'-CTAGCCGCCACTCACGTTGG-3'	This paper	N/A
sgRNA: eEF1A1/2-1: 5'-ATTTGAGAAGGAGGCTGCTG-3'	This paper	N/A
sgRNA: eEF1A1/2-2: 5'-GTTCGAGAAGGAGGCGGCTG-3'	This paper	N/A
sgRNAs for KMT Library: Table S1	This paper	N/A
Recombinant DNA		
Plasmid: lentiCRISPRv2	(Sanjana et al., 2014)	Addgene #52961
Plasmid: lentiCRISPRv2 hygro	A gift from Brett Stringer	Addgene #98291
Plasmid: psPAX2	Trono Lab Packaging and Envelope Plasmids	Addgene #12260
Plasmid: pMD2.G	Trono Lab Packaging and Envelope Plasmids	Addgene #12259
Plasmid: pCMV-dR8.2 dvpr	(Stewart et al., 2003)	AddGene #8455
Plasmid: pCMV-VSV-G	(Stewart et al., 2003)	Addgene #8454
Plasmid: pUMVC	(Stewart et al., 2003)	Addgene #8449
Plasmid: pBABE-neo	(Morgenstern and Land, 1990)	Addgene #1767
Plasmid: pWZL Blast GFP	(Orimo et al., 2005)	Addgene #12269
Plasmid: pGEX-6P-1	GE Healthcare	Cat# 28-9546-48
Plasmid: pcDNA3.1(+)	Thermo Fisher Scientific	Cat# V7020
Plasmid: pENTR3C	Thermo Fisher Scientific	Cat# A10465

REAGENT OR RESOURCE	SOURCE	IDENTIFIER
Plasmid: pLenti6.2 V5-DEST	Thermo Fisher Scientific	Cat# V36820
Software and Algorithms		
Prism 7	GraphPad	https://www.graphpad.com/; RRID:SCR_002798
Excel for Mac 2016	Microsoft	https://www.microsoft.com/en-us/; RRID:SCR_01613
Leica Application Suite X (LAS X)	Leica	https://www.leica-microsystems.com/ RRID:SCR_01
ImageJ – Fiji package	Freeware	http://fiji.sc; RRID:SCR_002285
Origin Pro 8	Microcal	https://www.originlab.com/ RRID:SCR_002815
Horos	GNU Lesser General Public License, Version 3.0	https://www.horosproject.org/
Other		
RPMI 1640 Medium	Corning	Cat# MT10017CV
DMEM Medium	Corning	Cat# MT10040CV
McCoy's Medium	Corning	Cat# MT10050CV
EMEM Medium	ATCC	Cat# 30-2003
Waymouth's Medium	Thermo Fisher Scientific	Cat# 11220035
Fetal bovine serum	Thermo Fisher Scientific	Cat# 10500056
PBS	Corning	Cat# MT21031CV
Trypsin-EDTA 0.25%	Corning	Cat# MT25053CI
PVDF membrane (0.2 μm)	BioRad	Cat# 1620177
PVDF membrane (0.45 μm)	Millipore	Cat# IPVH00010
Insulin-Transferrin-Selenium	Thermo Fisher Scientific	Cat# 41400045
Bovine Pituitary Extract (BPE)	Thermo Fisher Scientific	Cat# 13028014
Ethanolamine	Sigma-Aldrich	Cat# E6133
Nicotinamide	Sigma-Aldrich	Cat# N0636